Journal of Hydrology 530 (2015) 677–697

Contents lists available at ScienceDirect

Journal of Hydrology

journal homepage: www.elsevier.com/locate/jhydrol

Detection and attribution of non-stationarity in intensity and frequency of daily and 4-h extreme rainfall of Hyderabad, India

V. Agilan, N.V. Umamahesh *

Department of Civil Engineering, National Institute of Technology Warangal, Telangana 506004, India

ARTICLE INFO

Article history:
Received 1 June 2015
Received in revised form 16 September 2015
Accepted 9 October 2015
Available online 22 October 2015
This manuscript was handled by Andras Bardossy, Editor-in-Chief, with the assistance of Niko Verhoest, Associate Editor

Keywords:
ENSO cycle
Extreme rainfall
Global warming
Local temperature changes
Non-stationarity
Urbanization

SUMMARY

The high intensity rainfall has a significant contribution in urban area flooding and understanding this high intensity rainfall over urban areas may help us to reduce the damage caused by urban floods. In this study, the changes in Hyderabad city daily and sub-daily (4-h) extreme rainfall are analyzed using various climate change detection indices. Our analysis indicates that there is increasing trend in intensity and frequency of Hyderabad city daily extreme rainfall. In addition, increasing trend in intensity and frequency of monsoon months' (June–August) 1 a.m. to 4 a.m., 5 p.m. to 8 p.m. and 9 p.m. to 12 a.m. and non-monsoon months' 5 p.m. to 8 p.m. extreme rainfall is also observed. Based on recent theoretical development in the Extreme Value Theory (EVT), the changes in extreme rainfall of Hyderabad city are further attributed through modelling the non-stationarity (trend) present in the extreme rainfall intensity and frequency. The extreme rainfall intensity is modelled with peaks-over-threshold (POT) based Generalized Pareto Distribution (GPD) and frequency is modelled using inhomogeneous Poisson distribution. The trend is incorporated as covariate in the scale parameter (σ) of the GPD and the rate parameter (λ) of the Poisson distribution. In this study, four physical processes, i.e. Urbanization, El Niño-Southern Oscillation (ENSO) cycle, local temperature changes, and global warming are used as covariates. Further, the combinations of these covariates are also considered for modelling the non-stationarity.

Based on covariates and their combinations, fifteen non-stationary models and one stationary model are constructed and the best model is chosen based on the corrected Akaike Information Criterion (AICc) value. The covariate(s) in the best chosen non-stationary statistical model is/are attributed as the most significant physical process/processes which causes non-stationarity in the series. The study results indicate that the non-stationarity in daily extreme rainfall of Hyderabad city is mostly associated with global processes, i.e. ENSO cycle and global warming and the non-stationarity in sub-daily (4-h) extreme rainfall is mostly associated with local processes, i.e. Urbanization and local temperature changes. It is also observed that, in most of the cases, the stationary model is not even considerable based on AICc value.

1. Introduction

By 2030, towns and cities will be home to almost 5 billion people and it will be around 80% of the world population. The urban population of Africa and Asia will double in less than a generation (UNFPA, 2007). By the middle of 2009, for the first time, the population living in urban areas reached more than half of the world's population (DESA, 2010). At the same time, urban flooding and the damage to infrastructure and society are problems in both developing and developed countries. The high intensity (extreme) rainfall has a significant contribution in urban area flooding and the key challenge in urbanized area is to provide good quality detailed forecasts.

In addition, recent studies report that the frequency and intensity of extreme precipitation events are intensifying due to global climate change (Allen and Ingram, 2002; Trenberth et al., 2003; Emori and Brown, 2005; Cavanaugh et al., 2015; Xu et al., 2015). In specific, the impact of different climate processes on daily extreme precipitation has been analyzed, such as El Niño-Southern Oscillation (ENSO) cycle (Revadekar and Kulkarni, 2008; Kenyon and Hegerl, 2010; Zhang et al., 2010; Mondal and Mujumdar, 2015; Villafuerte and Matsumoto, 2015), global warming (Kunkel et al., 2013; Mondal and Mujumdar, 2015;

* Corresponding author. Tel.: +91 870 246 2112.
E-mail address: mahesh@nitw.ac.in (N.V. Umamahesh).

http://dx.doi.org/10.1016/j.jhydrol.2015.10.028
0022-1694/

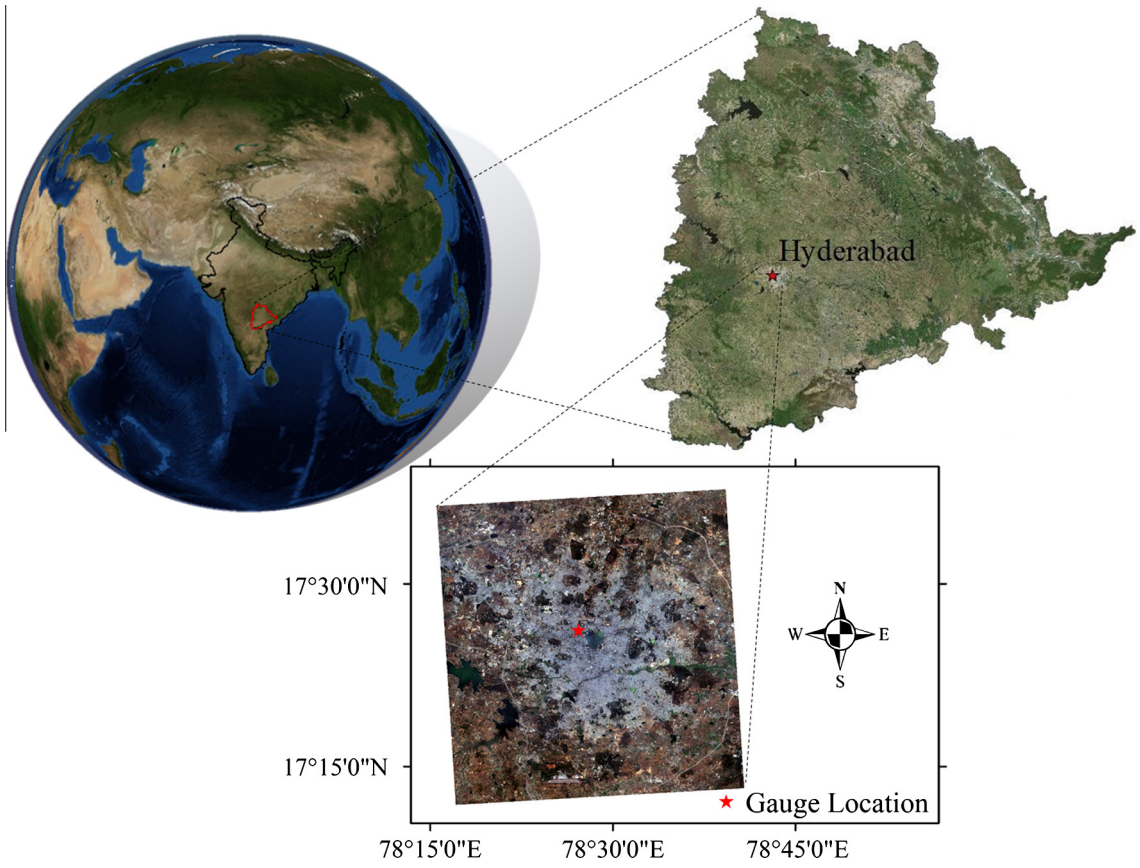

Fig. 1. Location map of Hyderabad city.

Villafuerte and Matsumoto, 2015). Furthermore, reasonable literature reported the possible changes in precipitation due to urbanization (Changnon et al., 1971; Shepherd et al., 2001; Shepherd and Burian, 2003; Burian and Shepherd, 2005; Lei et al., 2008; Kishtawal et al., 2009; Min et al., 2011; Zhang et al., 2014; Yang et al., 2015). Especially Burian and Shepherd (2005) hypothesized the possible role of urbanization in diurnal rainfall distribution. In addition, recent studies reported the influence of urbanization in extreme rainfall events as well (Lei et al., 2008; Miao et al., 2011). Thus, especially in urban areas, it is very important to understand how and why precipitation extremes have changed in the past and how they will change in the future.

In this study, the changes in daily and sub-daily (4-h) extreme rainfall intensity and frequency of Hyderabad city are analyzed. Further, positive trends in intensity and frequency of extreme rainfall are attributed through modelling the non-stationarity present in the series. In hydrology, usually, two approaches can be used to model the extreme values: block maxima and peaks over threshold (POT). The block maxima approach consists of modelling a sequence of maximum values taken from blocks of equal length, usually annual maximum. The probability distribution of values selected by this way converges asymptotically to the Generalized Extreme Value (GEV) distribution (Katz, 2013). But, the block maxima approach may miss real extreme events and the maximum value of some blocks may not be the extreme event. In addition, it is difficult to estimate the distribution parameters with small sample size. The POT approach utilizes the available data in a more efficient manner. POT selects all excesses over a given large threshold in each block. The asymptotic distribution of POT data set is the Generalized Pareto Distribution (GPD) (Coles, 2001; Katz, 2013). In case POT approach, some form of declustering is necessary to remove the temporal dependence within each extreme rainfall spell (Coles, 2001). The non-stationarity in the extreme values can be incorporated with both block maxima and POT approach. In this study, the POT approach is chosen because of its advantages over block maxima.

The non-stationarity present in the series can be modelled by incorporating covariates in parameters of the distribution (Katz et al., 2002; Khaliq et al., 2006; Katz, 2013). The covariate can be time (Sugahara et al., 2009; Cheng et al., 2014) or any independent physical processes, i.e. climate variables (Nogaj et al., 2007; Mondal and Mujumdar, 2015). In this study, four physical processes (i.e. Urbanization, ENSO cycle, local temperature changes, and global warming) and their combinations are used as covariates to model the non-stationarity present in the Hyderabad city daily and sub-daily (4-h) extreme rainfall intensity and frequency. The covariate(s) in the best chosen non-stationary statistical model is/are the most significant physical process/processes which causes non-stationarity in the series.

2. Study area

The Hyderabad city is the capital of the state of Telangana in India. Location map of the Hyderabad city is shown in Fig. 1. The Hyderabad city lies between latitude of 17.25°N and 17.60°N and longitude of 78.20°E and 78.75°E and situated at a height of about 500 m above the mean sea level. It is classified as a semi-arid region and the Köppen-Geiger classification is BSh (Peel et al., 2007). The major urbanization of Hyderabad city took place after 1990. During 1971–1990, the average rainfall of Hyderabad city was 796 mm per year. But, it has increased to 840 mm per year

Table 1
Satellite images used to model the urbanization.

Year	Satellite	Sensor	Date of accusation	Spatial resolution (m)
1972	Landsat-1	MSS	17-12-1972 (NASA, 1972)	60
1981	Landsat-3	MSS	14-10-1981 (NASA, 1981)	60
1989	Landsat-5	TM	22-02-1989 (NASA, 1989)	30
1994	Landsat-5	TM	25-04-1994 (NASA, 1994)	30
2000	Landsat-7	ETM+	29-02-2000 (NASA, 2000)	30
2003	Landsat-7	ETM+	20-01-2003 (NASA, 2003)	30
2006	Landsat-5	TM	10-04-2006 (NASA, 2006)	30
2010	Landsat-5	TM	21-04-2010 (NASA, 2010)	30
2013	Landsat-8	OLI-TIRS	25-12-2013 (NASA, 2013)	30

during 1991–2013. The wettest month of the city is August and the average rainfall of this month is 163 mm.

3. Data

3.1. Rainfall data

For this study, the hourly observed rainfall data for Hyderabad city is procured from the India Meteorological Department (IMD) for the period of 01-01-1971 to 31-12-2013 (43 years). This data is gauge observation and it is observed at the center of Hyderabad city i.e. 78.46°E and 17.45°N. The location of this gauge is given in Fig. 1 (star mark). Further, the current version of (V1101) APHRODITE gridded daily rainfall has been used to find the difference in urban rainfall with respect to non-urban rainfall and it is available at http://www.chikyu.ac.jp/precip/ for the period 1951–2007. APHRODITE is high resolution (0.25° longitude × 0.25° latitude) gridded daily rainfall data set which was developed for the Asian Regions under the Asian Precipitation Highly Resolved Observational Data Integration Towards Evaluation of the Water Resources (APHRODITE) project (Yatagai et al., 2012). The justification for using APHRODITE gridded daily rainfall is given in Section 4.2.

3.2. Covariates

The non-stationarity in the Hyderabad city extreme rainfall intensity and frequency is modelled with four physical processes (i.e. Urbanization, ENSO cycle, local mean temperature, and global warming) and their possible combinations. The data used to represent the four physical processes and justification to use them is given in this section.

3.2.1. Urbanization

In urban area, natural land surfaces are replaced with artificial surfaces that have different thermal properties (e.g., heat capacity and thermal inertia). Such surfaces are typically more capable of storing solar energy and converting it to sensible heat. As sensible heat is transferred to the air, the temperature of the air in urban areas tends to be 2–10 °C higher than surrounding non-urban areas (Shepherd et al., 2001). Thus, urban areas modify boundary layer processes through the creation of an Urban Heat Island (UHI) and the UHI can have a significant influence on mesoscale circulations and resulting convection (Shepherd et al., 2001). In the early 19th century, the issue about the influence of urbanization process on precipitation distribution was put forward (XiQuan et al., 2009). The initial investigation by Changnon et al. (1971) showed that the urbanization lead to increased precipitation during the summer months. In recent year, the possible changes in urban area rainfall due to urbanization have been analyzed by Burian and Shepherd (2005), Zhang et al. (2014) and Yang et al. (2015). Burian and Shepherd (2005) hypothesized the possible role of urbanization in diurnal rainfall distribution. Kishtawal et al. (2009) reported changes in extreme rainfall over India due to urbanization.

In this study, to know the urbanization pattern, the urban growth (growth in built-up land) of Hyderabad city from 1971 to 2013 is modelled using high resolution remote sensing data. In particular, the Level I (terrain information level (Anderson et al., 2001)) Land Use Land Cover (LULC) map is prepared with satellite images and used for identifying growth in built-up land. The Landsat satellite images are used to create Level I LULC maps of Hyderabad city to model the urban growth and it is worth to note that the Level I LULC map can be prepared with greater than 80% accuracy using satellite images (Avei and Akyurek, 2004).

The list of Landsat satellite images selected to model the Hyderabad city urban growth are listed in Table 1. The Maximum Likelihood Classification (MLC) algorithm is used to classify the satellite images. Because, the tolerance of the MLC algorithm to insufficient (less representative) training samples is high compared to other classification algorithms for Landsat images (Li et al., 2014) and it is often preferred by many remote sensing data users to classify land covers worldwide (Lu and Weng, 2007).

MLC algorithm is supervised pixel based image classification algorithm and it requires training samples of each class. Based on the preliminary analysis, four Level I classes are identified over the study area, i.e. Urban or Built-up Land, Water, Agricultural Land (Vegetation cover) and Barren Land. For each class minimum 5 training samples have been collected and merged. More details about the MLC algorithm can be obtained from Gibson and Power (2000).

Further, the class accuracy (Congalton and Green, 2009) is used to assess the accuracy of built-up land class. Based on 2013 extent of Hyderabad city, an area of 1913 km^2 is chosen and Landsat satellite images (Table 1) have been clipped for selected region and classified with the MLC algorithm. The steps involved in creating LULC map from Landsat satellite image is shown in Fig. 2. In Fig. 2, the four band multi spectral image is the Landsat satellite, blue, green, red and NIR band multi spectral image and the convergence is 80% class accuracy. The training samples are tuned until 80% class accuracy of built-up land class is achieved (see Table 2).

The Level I LULC maps prepared form Landsat images are shown in Fig. 4. From the LULC maps, the area of built-up land is calculated and the urban growth is modelled by an exponential function (Eq. (1)). The modelled urban growth is plotted in Fig. 3.

$$y = 6.322 \times 10^{-46} \times e^{(0.05485 \times x)} \quad (1)$$

Here, y is built-up land in square kilometer and x is corresponding year. This model (Eq. (1)) is valid only between 1971 and 2013. The

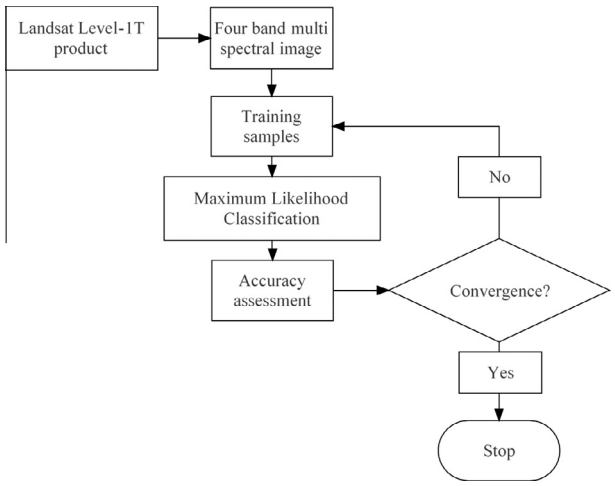

Fig. 2. Methodology of image classification.

Table 2
Satellite image classification results.

Year	Built-up land (km^2)	Percentage (%)	Class accuracy
1972	86.63	4.53	86.6
1981	104.89	5.48	86.36
1989	141.26	7.38	85.71
1994	180.41	9.43	97.22
2000	277.52	14.51	91.66
2003	313.02	16.36	91.52
2006	405.87	21.22	96.97
2010	479.07	25.04	94.93
2013	561.96	29.38	95.5

coefficient of determination (R^2) and RMSE of the model (Eq. (1)) is 0.992 and 16.35 respectively.

The built-up land area of each year between 1971 and 2013 is calculated using Eq. (1). As the urbanization follows the exponential function, it is unrealistic to use this modelled value directly. Thus, the modelled urbanization is first transformed using natural logarithm and used as the one of the covariate to model the characteristics of extreme precipitation of Hyderabad city.

3.2.2. El Niño-Southern Oscillation (ENSO) cycle

The ENSO cycle is the fluctuations in temperature between the ocean and the atmosphere in the east-central Equatorial Pacific (Zelle et al., 2004). In ENSO cycle, the cold phase is referred as La Niña and the warm phase is referred as El Niño. These deviations from normal surface temperatures can have large-scale impacts not only on ocean processes, but also on global weather and climate (Zelle et al., 2004). The ENSO cycle is the most important coupled ocean–atmosphere phenomenon to cause global climate variability on inter-annual time scales. The recent studies show the effect of ENSO cycle on extreme precipitation at local and regional scale (Kenyon and Hegerl, 2010; Zhang et al., 2010; Agilan and Umamahesh, 2015). Revadekar and Kulkarni (2008) studied the effect of ENSO cycle on extreme rainfall over India. Recently, Mondal and Mujumdar (2015) modelled the non-stationarity in intensity, duration and frequency of daily extreme rainfall over India with ENSO cycle as one of the covariate.

The ENSO cycle is represented by several ENSO indices such as Multivariate ENSO Index (MEI), Southern Oscillation Index (SOI) and Sea Surface Temperature (SST). Different studies use different ENSO indices to model the non-stationarity i.e. SOI (Katz et al., 2002), SST (Mondal and Mujumdar, 2015). Further, Revadekar and Kulkarni (2008) reported that the intensity and frequency of extreme precipitation in Southern India have strong correlation with NINO 3.4 SST anomalies 4–6 months in advance. In addition, some earlier studies reported that the MEI is better for monitoring ENSO than the SOI or various SST indices because the MEI integrates more information than other indices, it reflects the nature of the coupled ocean–atmosphere system better than either component, and it is less vulnerable to occasional data glitches in the monthly update cycles (Wolter and Timlin, 1998). Thus, MEI, SOI and SST are used as ENSO indicators with lag up to 12 months and the best ENSO indicator among them is chosen for monsoon and non-monsoon months and used for further analysis (refer Sections 5.3.1 and 5.4.1).

The ENSO index MEI is based on six main observed variables over the tropical Pacific i.e. sea-level pressure (P), zonal (U) and meridional (V) components of the surface wind, sea surface temperature (S), surface air temperature (A), and total cloudiness fraction of the sky (C). For this study, monthly MEI for the period of 1970–2013 is used and it is available at http://www.esrl.noaa.gov/psd/enso/mei/index.html (accessed on 01-04-2015). The SOI is a standardized index based on the observed sea level pressure differences between Tahiti and Darwin, Australia and it is available at http://www.cpc.ncep.noaa.gov/data/indices/soi (accessed on 01-04-2015). The more common SST index, i.e. monthly sea surface temperature anomaly over NINO 3.4 (17°E–120°W, 5°S–5°N) region with respect to 1981–2010 mean is used as a third ENSO indicator and it is available at http://www.cpc.ncep.noaa.gov/data/indices/sstoi.indices (accessed on 01-04-2015).

3.2.3. Global and local temperature anomaly

During the past century, human activities caused an increase in global temperature (Min et al., 2011; IPCC, 2013). The rising

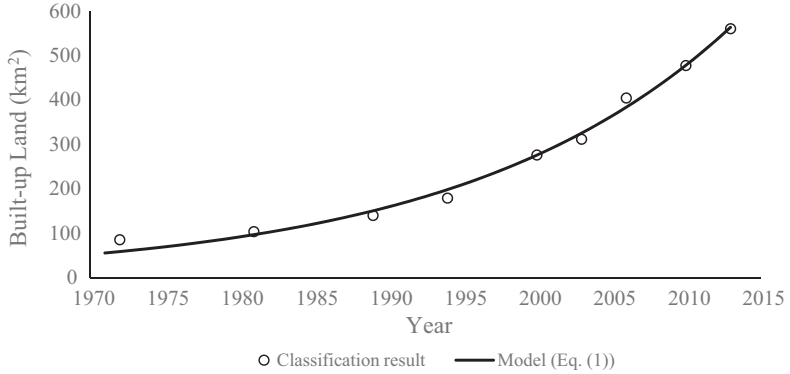

Fig. 3. Urban growth of Hyderabad city (1971–2013).

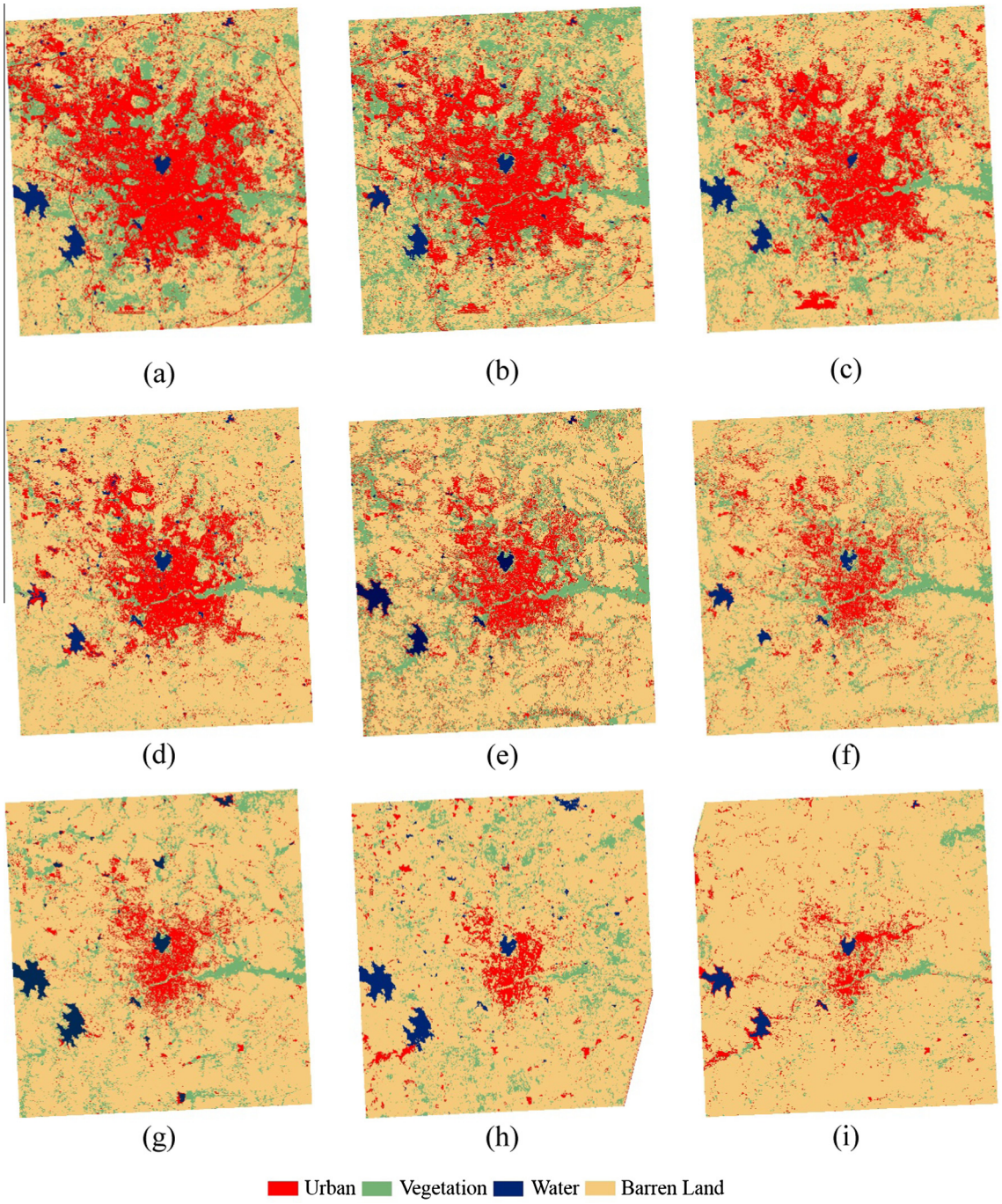

Fig. 4. Level I LULC map of (a) 2013, (b) 2010, (c) 2006, (d) 2003, (e) 2000, (f) 1994, (g) 1989, (h) 1981 and (i) 1972.

temperatures boost the atmosphere's water holding capacity by about 7% per 1 °C warming, thus directly affecting precipitation (Trenberth, 2011). And the recent studies show that the higher atmospheric water vapor can lead to more intense precipitation events (Berg et al., 2013; Kunkel et al., 2013). Furthermore, rising temperatures and subsequent increases in atmospheric moisture content may increase the probable maximum precipitation or the expected extreme precipitation (Kunkel et al., 2013). In addition, the physical mechanisms linking local temperatures with precipitation may not be the same as those linking global warming to extreme precipitation changes (Trenberth, 2011). In some part of India, the non-stationarity in intensity and frequency of extreme gridded rainfall is associated with local and global temperature anomaly (Mondal and Mujumdar, 2015). Hence, the choice of local and global temperatures as covariates for modelling non-stationarity in Hyderabad city extreme rainfall intensity and frequency is appropriate.

The hourly observed temperature data for Hyderabad city is procured from India Meteorological Department (IMD) for the period of 01-01-1971 to 31-12-2013 (43 years). This data is station observation and it is observed at the center of Hyderabad city i.e. 78.46°E and 17.45°N. The monthly mean temperature is calculated from the hourly temperature observations and the monthly Local Temperature Anomaly (LTA) based on 1971–2013 mean is

Table 3
ETCCDI for daily precipitation.

ID	Indicator name	Indicator definitions	Units
SDII	Simple Daily Intensity Index	The ratio of annual total precipitation to the number of wet days (> 1 mm)	mm/day
R10	Number of heavy precipitation days	Annual count when precipitation >10 mm	days
R20	Number of very heavy precipitation days	Annual count when precipitation >20 mm	days
CDD	Consecutive Dry Days	Maximum number of consecutive days when precipitation <1 mm	days
CWD	Consecutive Wet Days	Maximum number of consecutive days when precipitation >1 mm	days
R95p	Very wet days	Annual total precipitation from days >95th percentile	mm
R99p	Extremely wet days	Annual total precipitation from days >99th percentile	mm
PRCPTOT	Annual total wet-day precipitation	Annual total precipitation from days >1 mm	mm

calculated. The HadCRUT4 monthly observed Global Temperature Anomaly (GTA) with respect to the 1961–1990 mean is used as an indicator of global warming. The GTA is based on average surface air temperature observation and it is available at http://www.metoffice.gov.uk/hadobs/hadcrut4/ (accessed on 01-04-2015).

4. Change detection in extreme rainfall

4.1. Changes in daily extreme rainfall

The word "extreme" may refer to many different things in the climate literature and there is no unique climatological definition for extreme (Stephenson, 2008). But in the case of climate variable, such as precipitation, an extreme can be reasonably well defined referring to values in the tails of the distribution that would be expected to occur infrequently (Zeng and Zwires, 2013). In this section, the daily and sub-daily (4-h) precipitation extremes of Hyderabad city are analyzed. To address the needs of various aspects of climate research on extremes and to facilitate the monitoring of extremes, the Expert Team on Climate Change Detection and Indices (ETCCDI) defined a set of descriptive indices of extremes (Alexander et al., 2006; Zhang et al., 2011; Zeng and Zwires, 2013). In this study, the precipitation ETCCDI that are used to analyze the changes in daily extreme precipitation are listed in Table 3.

The variations in the above listed ETCCDI in each year are analyzed and fitted with linear regression and tested for statistical significance. The *F*-test is used to check the statistical significance of linear regression. The variation in Simple Daily Intensity Index (SDII) is shown in Fig. 5(a). Based on *F*-test, the linear fit of SDII is statistically significant. The SDII is following increasing trend. The SDII is the ratio between annual precipitation and number of wet days. Thus, the increasing trend in SDII indicates that the rainfall in wet days is increasing. In this study, the average wet days in a year is 65 days. The variation in R10 is plotted in Fig. 5(b). The linear fit of R10 is statistically insignificant, however, the slight increasing trend is noted from the linear fit of R10. In this study, 10 mm is the 73rd percentile daily rainfall. The variation in R20 is illustrated in Fig. 5(c). Based on *F*-test, the linear fit of R20 is statistically significant. In this study, 20 mm is the 87th percentile daily rainfall. From the linear fit of R20, it is noted that the frequency of high intensity rainfall has increased. The changes in Consecutive Dry Days (CDD) is plotted in Fig. 5(d). Slight decreasing trend is observed in the linear fit of CDD, but the fit is statistically insignificant. The average CDD of Hyderabad city is 100 days and it is based on time period 1971–2013. Fig. 5(e) shows the variation in Consecutive Wet Days (CWD). The linear fit of CWD shows the decreasing trend and it is statistically significant. From the variations of SDII and CWD, it is evident that the intensity of Hyderabad city daily rainfall is increasing. Based on time period 1971–2013, the average CWD of Hyderabad city is 7.4 days. The variation in high intensity rainfall, i.e. R95p is shown in Fig. 5(f). From the linear fit of R95p, it is seen that the high intensity rainfall is increasing and the linear fit is statistically significant. Increasing trend in R95p may be due to increase in frequency of high intensity rainfall or increase in magnitude (intensity) of high intensity rainfall. The 95th percentile daily rainfall of this study is 38.55 mm.

The variation in very high intensity rainfall, i.e. R99p is plotted in Fig. 5(g). Based on *F*-test, the linear fit of R99p is statistically significant. The linear fit of R99p shows an increasing trend. This also may be due to increase in frequency of very high intensity rainfall or increase in magnitude (intensity) of very high intensity rainfall. The 99th percentile daily rainfall of this study is 71.625 mm. The variation in annual total wet-day precipitation (PRCPTOT) is shown in Fig. 5(h). The linear fit of PRCPTOT shows the increasing trend and the linear fit is statistically significant. From the variations in 8 indices (Table 3), it is clear that the intensity and (or) frequency of Hyderabad city daily extreme rainfall has increased. But it is not clear that during a day when it is increased. Thus, the change detection study is further extended.

4.2. Change in diurnal rainfall distribution

Burian and Shepherd (2005) analyzed the effect of urbanization on the diurnal rainfall pattern in Houston, USA. They compared pre and post urban rainfall patterns and reported that the diurnal rainfall distribution has changed, especially in noon to 4 p.m. and 4 p.m. to 8 p.m. Houston is a coastal city and located in USA but our study area is a non-coastal city and located in India. The diurnal rainfall pattern may be different for the current study area. The similar study has been conducted to detect the changes in the diurnal rainfall distribution of Hyderabad city. As the hourly rainfall record before 1971 is not available for Hyderabad city, two time periods after 1971 i.e. 1971–1980 and 2004–2013 are chosen to detect the changes in diurnal distribution. Between 1980 and 2013, there is around 25% increase (refer Section 3.2.1) in urban built up land.

The impact of urbanization in rainfall is more during the warm season, i.e. June–August (Changnon et al., 1971; Burian and Shepherd, 2005; Zhang et al., 2009). But there is variability associated with Indian rainfall (Krishnamurthy and Shukla, 2000). Hence, to find the difference in monthly rainfall distribution in urban area, the variation of monthly rainfall distribution of urban area is compared with non-urban area monthly rainfall distribution. The APHRODITE gridded daily rainfall has been used to analyze the difference between urban and non-urban area monthly rainfall distribution. APHRODITE is high resolution daily rainfall data set (Yatagai et al., 2012) and studies conducted comparing daily rainfall estimates from APHRODITE with those from the Indian Meteorological Department's (IMD) rain gauges indicated a high correlation (Indu and Kumar, 2014). Further, Rajeevan and Bhate (2009) carried a quantitative analysis of this product over India and reported a difference of less than 3 mm/day. Four APHRODITE data set grids represent the Hyderabad city. However, a most urbanized grid in the Hyderabad city and one non-urban grid point attached to the Hyderabad city grid are chosen for this study. The average monthly rainfall is calculated from daily APHRODITE rainfall and the average monthly rainfall distribution of urban area

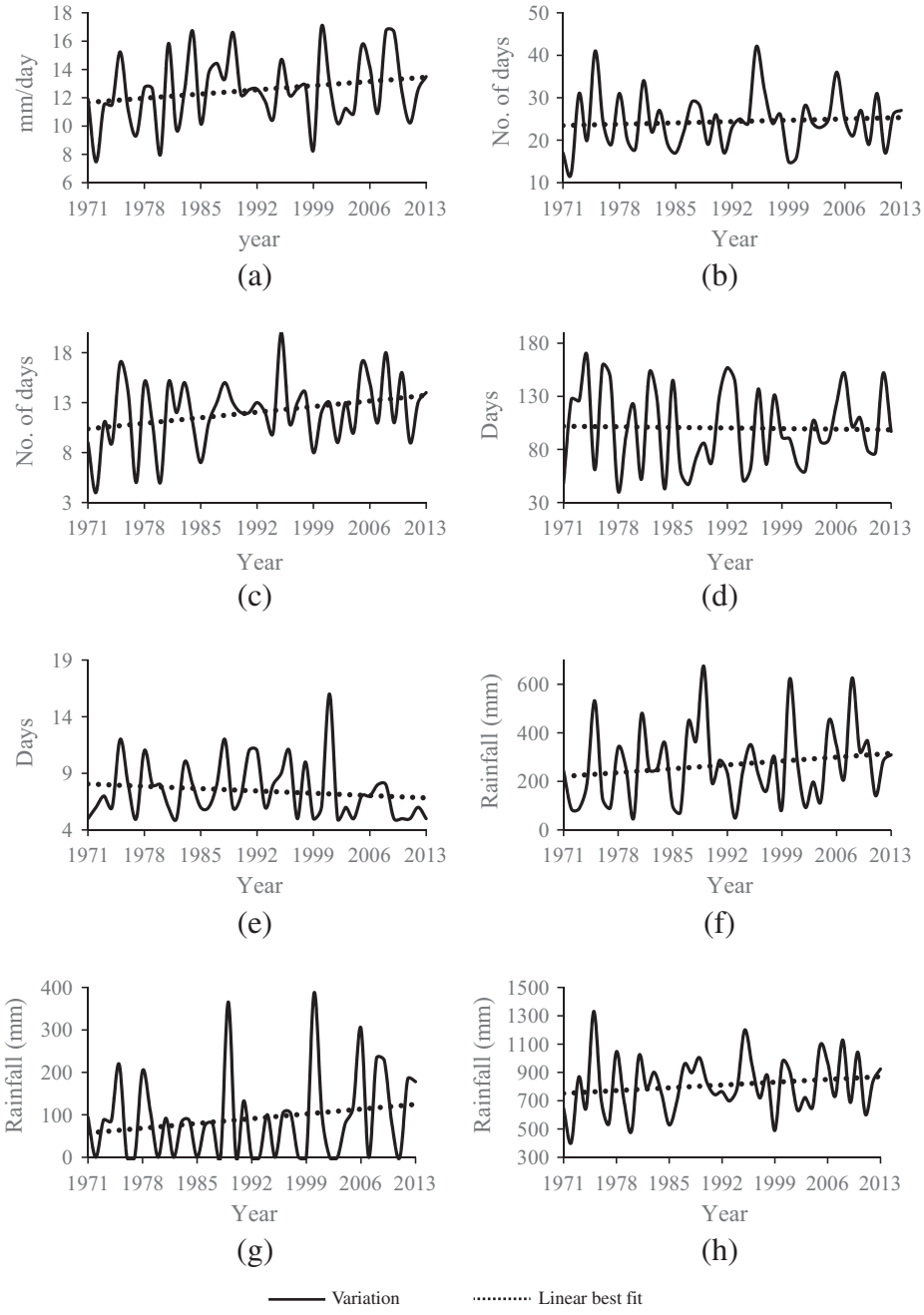

Fig. 5. Variations in (a) SDII, (b) R10, (c) R20, (d) CDD, (e) CWD, (f) R95p, (g) R99p and (h) PRCPTOT of daily rainfall of Hyderabad city and linear best fit of the variation (dashed lines).

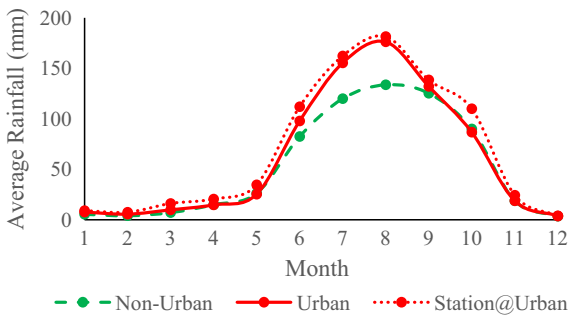

Fig. 6. Average monthly rainfall distribution of urban and non-urban area.

and non-urban area are plotted in Fig. 6. In addition, the monthly rainfall distribution of urban area is analyzed with IMD station observation and plotted in Fig. 6 and these plots are based on 1971–2007 time period.

From the variations in average monthly rainfall distribution, it is clear that the average monthly rainfall in urban area is different during June–August when compared to non-urban area. In India, June–August is often referred as monsoon months. Hence, the diurnal rainfall distribution of monsoon months and non-monsoon months (except June–August) are analyzed separately.

As Burian and Shepherd (2005) divided the day into 4-h time increments (i.e. midnight to 4 a.m., 4 a.m. to 8 a.m., and so on) to study the diurnal rainfall distribution of Houston (USA), the same approach has been followed to analyze the changes in the diurnal

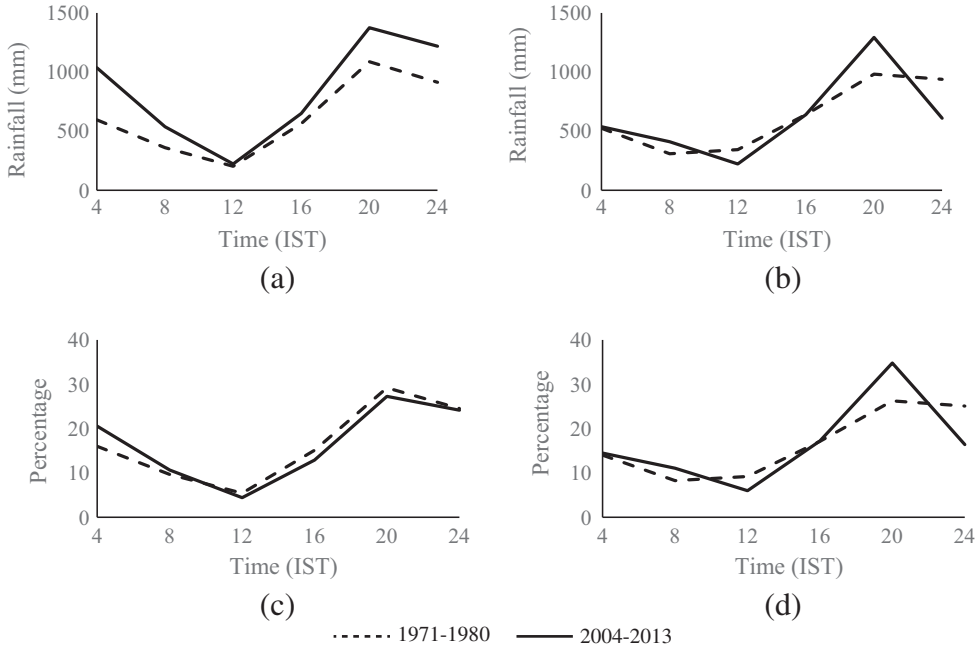

Fig. 7. Diurnal rainfall distribution of (a) monsoon months, (b) non-monsoon months and diurnal rainfall percentage distribution of (c) monsoon months, (d) non-monsoon months.

Table 4
ETCCDI for 4 h precipitation.

ID	Indicator name	Indicator definitions	Units
R10-4 h	Number of heavy 4 h precipitation	Annual count when precipitation >10 mm during corresponding 4 h and season	days
R20-4 h	Number of very heavy 4 h precipitation	Annual count when precipitation >20 mm during corresponding 4 h and season	days
R95p-4 h	Very wet 4 h	Annual total precipitation from days >95th percentile rainfall of corresponding 4 h and season	mm
PRCPTOT-4 h	Annual total wet 4 h precipitation	Annual total precipitation from days >1 mm during corresponding 4 h and season	mm

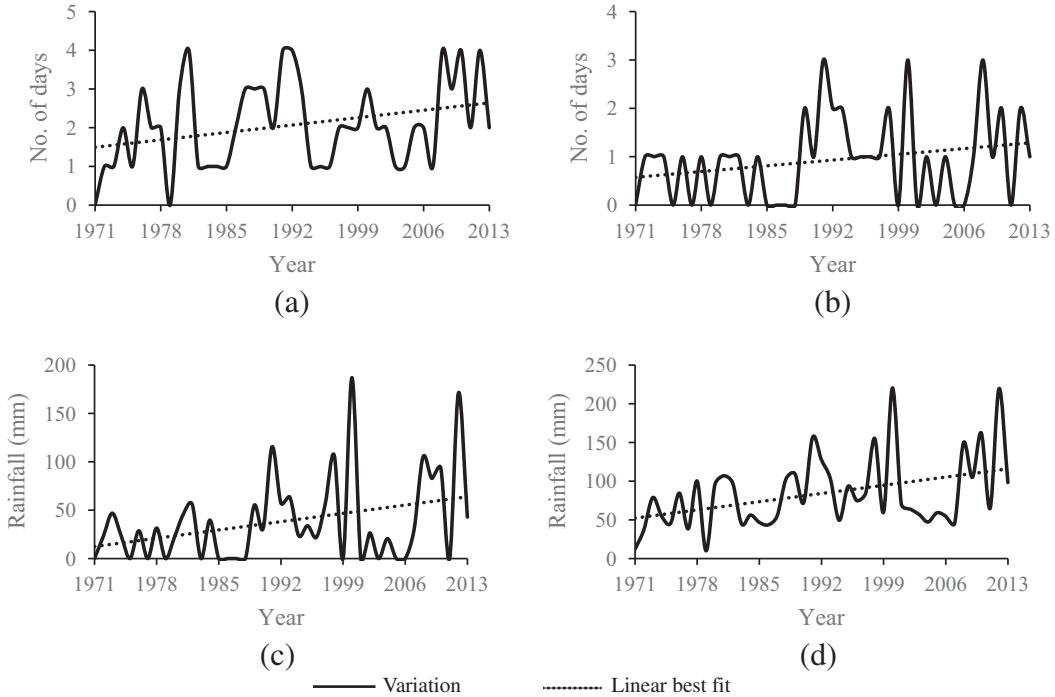

Fig. 8. Variations in (a) R10-4 h, (b) R20-4 h, (c) R95-4 h and (d) PRCPTOT-4 h of monsoon 1 a.m. to 4 a.m. rainfall and linear best fit of the variation (dashed lines).

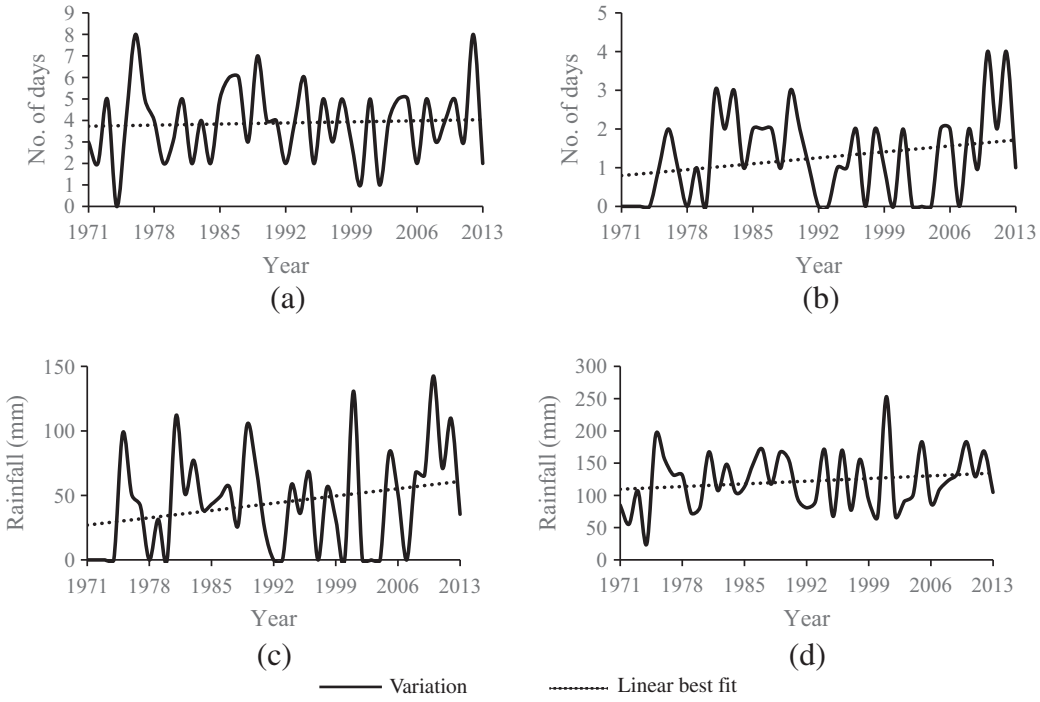

Fig. 9. Variations in (a) R10-4 h, (b) R20-4 h, (c) R95-4 h and (d) PRCPTOT-4 h of monsoon 5 p.m. to 8 p.m. rainfall and linear best fit of the variation (dashed lines).

rainfall distribution of Hyderabad. The diurnal rainfall distribution of monsoon and non-monsoon months are shown in Fig. 7 (a) and (b) and the diurnal rainfall percentage distribution of monsoon and non-monsoon months are shown in Fig. 7(c) and (d). From the diurnal rainfall and percentage distribution, it is clear that the diurnal rainfall distribution of both monsoon and non-monsoon months have changed significantly between 1971–1980 and 2004–2013.

During the monsoon months, except 9 a.m. to 12 p.m., the rainfall that occurred in other 4-h time periods have increased after urbanization and it may be due to the increasing trend in total rainfall (refer Section 4.1). But the diurnal rainfall percentage distribution confirms that the percentage rainfall occurring between 1 a.m. and 4 a.m. has increased by 4.5% and nearly 1% increase in percentage rainfall that occurred between 5 a.m. and 8 a.m. Apart from this, the percentage of rainfall that occurred in all other time periods has decreased during monsoon months. The maximum decrease in percentage rainfall occurrence during monsoon months is 2.22% and it is during 1 p.m. to 4 p.m.

From Fig. 7(a)–(d), it is noted that the change in the diurnal rainfall distribution of non-monsoon months is significantly different from monsoon months. Fig. 7(b) shows that the rainfall that occurred during non-monsoon months' 5 a.m. to 8 a.m. and 5 p.m. to 8 p.m. has increased significantly. But, 9 a.m. to 12 p.m. and 9 p.m. to 12 a.m. rainfall has significantly decreased and it is noted that there is no significant change in rainfall occurrence during 1 a.m. to 4 a.m. and 1 p.m. to 4 p.m. Fig. 7(d) reveals the diurnal rainfall percentage distribution of non-monsoon months and maximum of 8.52% increase in percentage rainfall that occurred between 5 p.m. and 8 p.m. and maximum of 8.67% decrease in percentage rainfall that occurred between 9 p.m. and 12 a.m. is observed.

From the analysis of results, it is evident that the rainfall occurring during 1 a.m. to 4 a.m., 5 p.m. to 8 p.m. and 9 p.m. to 12 a.m. have increased significantly in the monsoon months. During non-monsoon months the rainfall that occurred between 5 p.m. and 8 p.m. has increased significantly. However, it is not clear that the extreme rainfall that occurred during these periods have changed or not. To examine the changes in extreme rainfall of these 4 h time periods, some of the ETCCDI of daily precipitation (Table 3) have been modified for 4 h rainfall and given in Table 4.

4.2.1. Changes in monsoon months' 1 a.m. to 4 a.m. extreme rainfall

The modified ETCCDI listed in Table 4 are used to analyze the changes in the monsoon months' 1 a.m. to 4 a.m. extreme rainfall. The variations and linear best fit of R10-4 h, R20-4 h, R95p-4 h and PRCPTOT-4 h are plotted in Fig. 8(a)–(d) respectively. During this period, the 10 mm/4 h is the 89th percentile rainfall and 20 mm/4 h is 96th percentile rainfall. 19.345 mm/4 h is the 95th percentile rainfall of the period. Increasing trend in R95p-4 h may be due to increase in frequency of high intensity rainfall or increase in magnitude (intensity) of high intensity rainfall. All four ETCCDI of monsoon months' 1 a.m. to 4 a.m. rainfall are having statistically significant increasing trend and it indicates that the extreme rainfall that occurred between 1 a.m. and 4 a.m. during monsoon months has increased.

4.2.2. Changes in monsoon months' 5 p.m. to 8 p.m. extreme rainfall

The extreme rainfall occurring between 5 p.m. and 8 p.m. during monsoon months is analyzed with 4-h extreme rainfall ETCCDI (Table 4). The variations and linear best fit of R10-4 h, R20-4 h, R95p-4 h and PRCPTOT-4 h are plotted in Fig. 9(a)–(d) respectively. The linear fits of all four indices are having increasing trend and except the linear fit of R10-4 h, all other linear fits are statistically significant. During this period 10 mm/4 h is the 86th percentile rainfall, 20 mm/4 h is 96th percentile rainfall and 19.69 mm/4 h is the 95th percentile rainfall of the period. The increasing trend in linear fits indicate that the extreme rainfall occurring between 5 p.m. and 8 p.m. during monsoon months has also increased.

4.2.3. Changes in monsoon months' 9 p.m. to 12 a.m. extreme rainfall

Fig. 10 shows the variations in 4-h ETCCDI (Table 4) of extreme rainfall that occurred between 9 p.m. and 12 a.m. during monsoon months. Similar to previous time period (i.e. 5 p.m. to 8 p.m.)

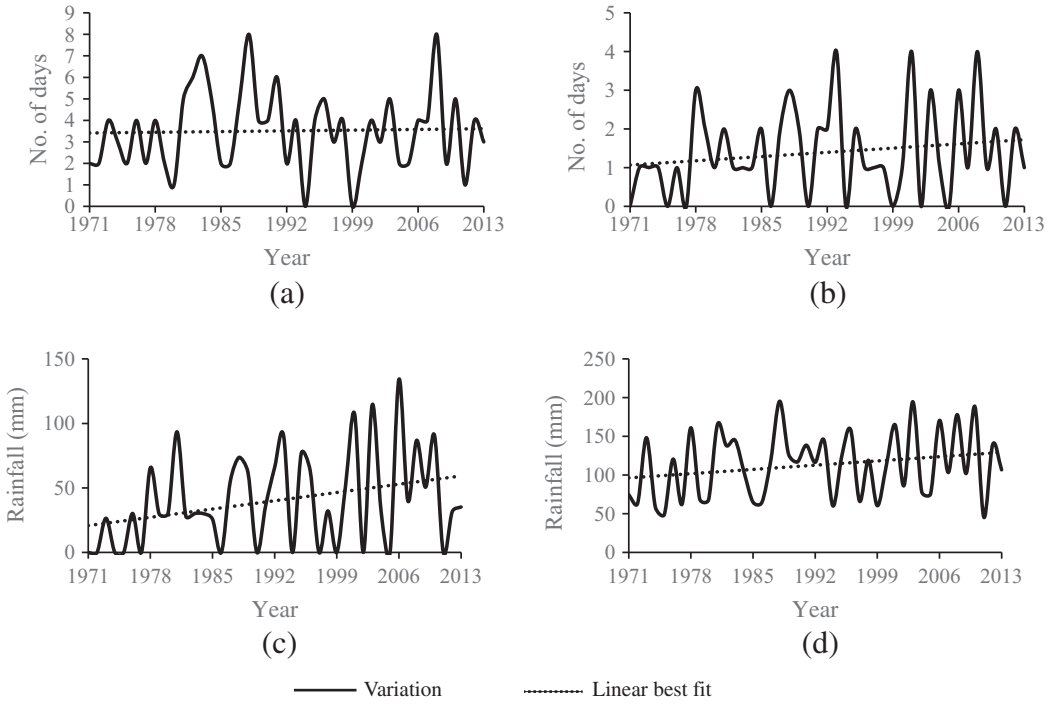

Fig. 10. Variations in (a) R10-4 h, (b) R20-4 h, (c) R95-4 h and (d) PRCPTOT-4 h of monsoon 9 p.m. to 12 a.m. rainfall and linear best fit of the variation (dashed lines).

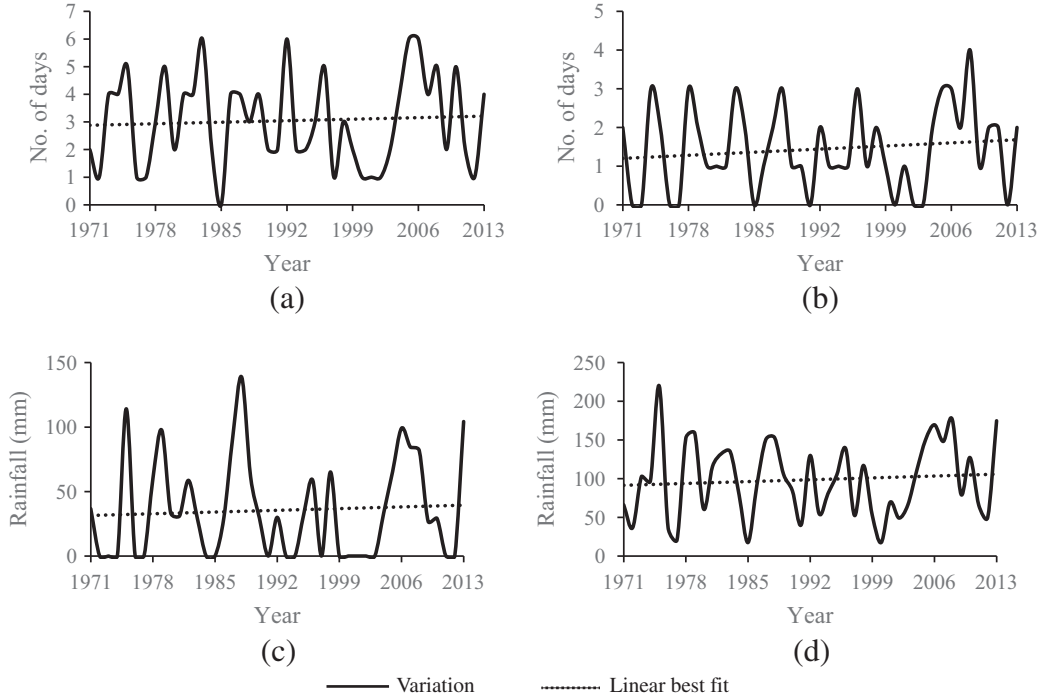

Fig. 11. Variations in (a) R10-4 h, (b) R20-4 h, (c) R95-4 h and (d) PRCPTOT-4 h of non-monsoon 5 p.m. to 8 p.m. rainfall and linear best fit of the variation (dashed lines).

results, the linear fits of all four indices are having increasing trend and they are statistically significant except the linear fit of R10-4 h. Based on rainfall that occurred between 9 p.m. and 12 a.m. time period of monsoon months, 10 mm/4 h is the 85th percentile rainfall, 20 mm/4 h is 93rd percentile rainfall and 23.345 mm/4 h is the 95th percentile rainfall. It is noted that the intensity of high percentile rainfall that occurred between 9 p.m. and 12 a.m. is comparatively higher than rainfall that occurred between 1 a.m. to 4 a.m. and 5 p.m. to 8 p.m. and the increasing trend in linear fits indicate that the extreme rainfall that occurred between 9 p.m. and 12 a.m. during monsoon months has increased.

During the monsoon months, the extreme rainfall frequency and intensity that occurred between 1 a.m. to 4 a.m., 5 p.m. to 8 p.m. and 9 p.m. to 12 a.m. have increased. The increasing trend of 1 a.m. to 4 a.m. extreme rainfall is steeper than other two time periods and the intensity of rainfall that occurred between 9 p.m. and 12 a.m. is comparatively higher than other time periods. These increasing trends could be due to one or more physical process.

Table 5
List of GPD and Poisson models constructed in this study and their specifications.

GPD model		Poisson model	
ID	Specification	ID	Specification
GPD-1	$Y \sim \mathrm{GP}(\sigma_0, \xi)$	P-1	$F \sim P(e^{(\lambda_0)})$
GPD-2	$Y \sim \mathrm{GP}(e^{(\sigma_0+\sigma_1 U)}, \xi)$	P-2	$F \sim P(e^{(\lambda_0+\lambda_1 U)})$
GPD-3	$Y \sim GP(e^{(\sigma_0+\sigma_1 \mathrm{LTA})}, \xi)$	P-3	$F \sim P(e^{(\lambda_0+\lambda_1 \mathrm{LTA})})$
GPD-4	$Y \sim GP(e^{(\sigma_0+\sigma_1 \mathrm{GTA})}, \xi)$	P-4	$F \sim P(e^{(\lambda_0+\lambda_1 \mathrm{GTA})})$
GPD-5	$Y \sim GP(e^{(\sigma_0+\sigma_1 E)}, \xi)$	P-5	$F \sim P(e^{(\lambda_0+\lambda_1 E)})$
GPD-6	$Y \sim GP(e^{(\sigma_0+\sigma_1 U+\sigma_2 \mathrm{LTA})}, \xi)$	P-6	$F \sim P(e^{(\lambda_0+\lambda_1 U+\lambda_2 \mathrm{LTA})})$
GPD-7	$Y \sim GP(e^{(\sigma_0+\sigma_1 U+\sigma_2 \mathrm{GTA})}, \xi)$	P-7	$F \sim P(e^{(\lambda_0+\lambda_1 U+\lambda_2 \mathrm{GTA})})$
GPD-8	$Y \sim GP(e^{(\sigma_0+\sigma_1 U+\sigma_2 E)}, \xi)$	P-8	$F \sim P(e^{(\lambda_0+\lambda_1 U+\lambda_2 E)})$
GPD-9	$Y \sim GP(e^{(\sigma_0+\sigma_1 \mathrm{LTA}+\sigma_2 \mathrm{GTA})}, \xi)$	P-9	$F \sim P(e^{(\lambda_0+\lambda_1 \mathrm{LTA}+\lambda_2 \mathrm{GTA})})$
GPD-10	$Y \sim GP(e^{(\sigma_0+\sigma_1 \mathrm{LTA}+\sigma_2 E)}, \xi)$	P-10	$F \sim P(e^{(\lambda_0+\lambda_1 \mathrm{LTA}+\lambda_2 E)})$
GPD-11	$Y \sim GP(e^{(\sigma_0+\sigma_1 \mathrm{GTA}+\sigma_2 E)}, \xi)$	P-11	$F \sim P(e^{(\lambda_0+\lambda_1 \mathrm{GTA}+\lambda_2 E)})$
GPD-12	$Y \sim GP(e^{(\sigma_0+\sigma_1 U+\sigma_2 \mathrm{LTA}+\sigma_3 \mathrm{GTA})}, \xi)$	P-12	$F \sim P(e^{(\lambda_0+\lambda_1 U+\lambda_2 \mathrm{LTA}+\lambda_3 \mathrm{GTA})})$
GPD-13	$Y \sim GP(e^{(\sigma_0+\sigma_1 U+\sigma_2 \mathrm{LTA}+\sigma_3 E)}, \xi)$	P-13	$F \sim P(e^{(\lambda_0+\lambda_1 U+\lambda_2 \mathrm{LTA}+\lambda_3 E)})$
GPD-14	$Y \sim GP(e^{(\sigma_0+\sigma_1 U+\sigma_2 \mathrm{GTA}+\sigma_3 E)}, \xi)$	P-14	$F \sim P(e^{(\lambda_0+\lambda_1 U+\lambda_2 \mathrm{GTA}+\lambda_3 E)})$
GPD-15	$Y \sim GP(e^{(\sigma_0+\sigma_1 \mathrm{LTA}+\sigma_2 \mathrm{GTA}+\sigma_3 E)}, \xi)$	P-15	$F \sim P(e^{(\lambda_0+\lambda_1 \mathrm{LTA}+\lambda_2 \mathrm{GTA}+\lambda_3 E)})$
GPD-16	$Y \sim GP(e^{(\sigma_0+\sigma_1 U+\sigma_2 \mathrm{LTA}+\sigma_3 \mathrm{GTA}+\sigma_4 E)}, \xi)$	P-16	$F \sim P(e^{(\lambda_0+\lambda_1 U+\lambda_2 \mathrm{LTA}+\lambda_3 \mathrm{GTA}+\lambda_4 E)})$

Note: F – Frequency; P – Poisson distribution.

4.2.4. Changes in non-monsoon months' 5 p.m. to 8 p.m. extreme rainfall

During non-monsoon months, the amount of rainfall that occurred between 5 p.m. and 8 p.m. has increased around 8.5% and it may be from normal rainfall and/or extreme rainfall. Thus, the variations in 4 h rainfall extreme indices of this time period are analyzed and plotted in Fig. 11. The linear fit of extreme rainfall indices R10-4 h, R95-4 h and PRCPTOT-4 h are having increasing trend and they are statistically insignificant. But, the linear fit of R20-4 h is having increasing trend and it is statistically significant. Based on rainfall that occurred between 5 p.m. and 8 p.m. time period of non-monsoon months, 10 mm/4 h is the 83rd percentile rainfall, 20 mm/4 h is 92nd percentile rainfall and 26.6 mm/4 h is the 95th percentile rainfall. The increasing trend in linear fits indicate that the extreme rainfall that occurred between 5 p.m. and 8 p.m. during non-monsoon months has also increased.

Based on analysis of results, significant changes in daily and 4-h extreme precipitation occurred during monsoon months and non-monsoon months are observed. For further analysis, the monsoon months' 1 a.m. to 4 a.m., 5 p.m. to 8 p.m. and 9 p.m. to 12 a.m. and non-monsoon months' 5 p.m. to 8 p.m. rainfall are considered along with the monsoon and non-monsoon months' daily rainfall.

5. Attribution through modelling non-stationarity

Though it is important to detect the changes in extreme rainfall, attributing possible cause for the change is very important to understand the future behavior of the extreme. Just because the changes are detected in urban area, it is unrealistic to attribute urbanization as a cause for the changes. In this section, the possible cause(s) for the changes in Hyderabad city extreme rainfall intensity and frequency are attributed through modelling non-stationarity in the extreme rainfall intensity and frequency. The intensity and frequency of POT rainfall series can be modelled simultaneously through Point Process approach (Katz, 2013). However, it is still not commonly used to model trend (non-stationarity) in climate or hydrological extremes (Katz, 2013). Thus, the more common Poisson-GP approach (Katz, 2013) is used to model the non-stationarity in extreme rainfall intensity and frequency. In particular, the intensity of extreme rainfall is modelled with non-stationary Generalized Pareto (GP) distribution and frequency of extreme rainfall is modelled with inhomogeneous Poisson distribution.

5.1. Modelling non-stationarity in intensity of extreme rainfall

5.1.1. GPD model

Consider a sequence of M independent and identically distributed (iid) random variable $X_1, X_2, \ldots, X_M$ conditioned on $X > u$, where u is a given high threshold. For sufficiently high threshold (u), the excesses $Y = X - u$ converges to GPD and it is given by Eq. (2) (Coles, 2001; Khaliq et al., 2006).

$$F(y,\sigma,\xi) = P(X \leqslant u + y | X \geqslant u) = \begin{cases} 1 - \left[1 + \frac{y}{\sigma}\xi\right]^{-1/\xi}, & \sigma > 0,\ 1 + \frac{y}{\sigma}\xi > 0 \\ 1 - \exp\left(\frac{-y}{\sigma}\right), & \sigma > 0,\ \xi = 0 \end{cases} \tag{2}$$

where σ and ξ are the scale and shape parameters respectively. The scale parameter σ is the function of chosen threshold u and it characterizes the spread of the distribution. As the precise estimation of shape parameter is difficult, it is unrealistic to assume it as a smooth function of time (Coles, 2001). Thus, the shape parameter is kept constant and the non-stationarity is introduced only in scale parameter σ. The general form of non-stationary setting for the shape parameter of GPD as a function of physical covariates is given by Eq. (3).

$$\begin{aligned} \sigma(i) &= \exp(\sigma_0 + \sigma_1 c_1 + \sigma_2 c_2 + \sigma_3 c_3 + \sigma_4 c_4) \\ \xi(i) &= \xi \end{aligned} \tag{3}$$

where i denotes the day or 4-h; c_1, c_2, c_3 and c_4 are physical covariates i.e. Urbanization (U), ENSO cycle (E), GTA and LTA. For the stationary GPD, the physical covariates c_1, c_2, c_3 and c_4 values are zero. The exponential function in Eq. (3) ensure the positive value of the scale parameter. The slope parameters σ_1, σ_2, σ_3 and σ_4 represent the trend due to the effect of covariates c_1, c_2, c_3 and c_4 respectively. Apart from stationary model, based on four covariates and their combinations, fifteen non-stationary models are constructed (refer Table 5). The physical covariate(s) of the best GPD model is/are the most significant physical process/processes which is/are responsible for the change in intensity of extreme rainfall.

5.1.2. Threshold selection

The next critical step is to select an adequate threshold value that preserves the asymptotic property of the GPD. i.e. too low a threshold is likely to violate the asymptotic basis of the model, leading to bias; too high a threshold will generate few excesses which may lead to high variance in the model estimate. The standard practice is to adopt as low a threshold as possible, subject to the limit model providing a reasonable approximation (Coles,

Table 6
MRL selected threshold values for different rainfall.

Rainfall	Threshold in mm (Percentile)	Number of exceedance (after declustering)
Daily – monsoon months	38.57 (95)	106 (99)
Daily – non-monsoon months	38.49 (95)	84 (79)
Monsoon months – 1 a.m. to 4 a.m.	12.083 (91)	74 (60)
Monsoon months – 5 p.m. to 8 p.m.	17 (94)	66 (58)
Monsoon months – 9 p.m. to 12 a.m.	16.856 (92)	77 (66)
Non-monsoon months – 5 p.m. to 8 p.m.	16.4 (90)	76 (76)

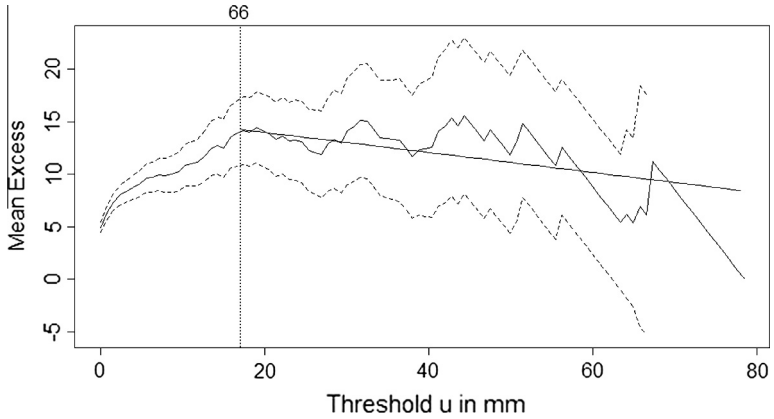

Fig. 12. MRL plot for monsoon 5 p.m. to 8 p.m. rainfall. Solid and dashed jagged lines are MRL and 95% confidence intervals respectively. The sloping down straight line is MRL implied by ML parameter estimates for threshold $u = 17$ mm. Vertical dashed lines indicates threshold and its exceedance.

2001). A number of procedures for selecting thresholds have been proposed in the literature, but there is no universally accepted rule for it (Scarrott and MacDonald, 2012). In this study, the threshold values for different rainfall are interpreted through MRL plot and are given in Table 6. For more information about MRL plot, the interested reader is referred to Coles (2001). The MRL plot for monsoon months' 5 p.m. to 8 p.m. rainfall is shown in Fig. 12. For brevity, the MRL plots of other rainfall are not shown in this paper.

Further, to remove the temporal dependence within each extreme rainfall spell, some form of declustering is necessary (Coles, 2001). An extreme rainfall cluster is consecutive days when rainfall is higher than u and these clusters are separated from each other by one or more days when rainfall is lower than u. Then the clustered extreme rainfall is declustered by retaining only maximum extreme rainfall in each cluster. In case of 4-h rainfall, the non-monsoon months' 9 p.m. to 12 a.m. extreme rainfall is automatically separated by 20 h or more. But, monsoon months' 1 a.m. to 4 a.m., 5 p.m. to 8 p.m. and 9 p.m. to 12 a.m. may have temporal dependency because it is a continuous time period i.e. 5 p.m. to 4 a.m. (next day). In these three 4-h time period, if two or three continuous 4-h time period have rainfall intensity more than corresponding 4-h threshold, the maximum among them is selected and remaining one/two 4-h extreme rainfall is/are removed.

5.1.3. Parameter estimation

Once the threshold is selected and extreme rainfall series is declustered, the parameters of the GP distribution can be estimated by the method of maximum likelihood. Because the method of maximum likelihood can be easily extended to the non-stationary case (Coles, 2001; Katz, 2013). Let the values $Y = y_1, y_2 \ldots, y_n$ are the n excesses of a threshold u. The log likelihood derived from Eq. (2) is given as

$$L(\sigma,\xi|Y) = -n\log\sigma - (1+1/\xi)\sum_{i=1}^{n}\log(1+\xi y_i/\sigma),\ (1+\xi y_i/\sigma) > 0,\ \xi \neq 0$$
$$L(\sigma|Y) = -n\log\sigma - 1/\sigma\sum_{i=1}^{n} y_i,\ \xi = 0 \quad (4)$$

For non-stationary case, the scale parameters σ in the above equation is replaced with Eq. (3). Minimization of negative log likelihood ($-L(\beta/Y)$; $\beta = (\sigma,\xi)$) through Nelder–Mead (Nelder and Mead, 1965) optimization method is adopted to estimate the parameters (Coles, 2001). The maximum likelihood estimation is not recommended when the n is less than 25. Because it estimates physically infeasible shape parameter values for small samples (Martins and Stedinge, 2001; Sugahara et al., 2009).

5.1.4. Identification of the best model

The Akaike Information Criterion (AIC), which penalizes the minimized $-L(\beta/Y)$ for the number of parameters estimated, can be used to select the best model (Katz, 2013). In this study, the small-sample version of AIC, called corrected Akaike Information Criterion (AICc), is used to select the best model among several non-stationary models and one stationary model. The AICc is recommended in practical application because it outperforms AIC, in such way that it helps in avoiding over fitting the data more than conventional AIC (Sugahara et al., 2009). If a candidate model with k parameters, β, fitted to a sample of n exceedances of threshold u, then the AICc of the model is as follows

$$\mathrm{AICc} = -2L(\beta|Y) + 2k + \frac{2k(k+1)}{n-k-1} \quad (5)$$

where $-L(\beta/Y)$ is the minimized negative log likelihood function. The first two terms of AICc are same as conventional AIC and AICc converges to AIC if n gets large. In addition, the rescaled form of AICc i.e. Δ_i (Burnham and Anderson, 2004) is used to rank the non-stationary models and given in Eq. (6).

$$\Delta_i = \mathrm{AICc} - \min(\mathrm{AICc}) \quad (6)$$

where min(AICc) is the smallest AICc among all the models. The model which has Δ_i value zero is the best model and the models having $\Delta_i \leqslant 2$ are considered reasonable choices (Burnham and Anderson, 2004).

Table 7
Non-stationary GPD models' performance for **monsoon daily** extreme rainfall with different ENSO indices as covariate.

S. no.	MEI	AICc	S. no.	SOI	AICc	S. no.	SST	AICc
1	MEI-0	836.77	14	SOI-0	836.76	27	SST-0	836.67
2	MEI-1	836.92	15	SOI-1	836.53	28	SST-1	836.62
3	MEI-2	836.81	16	SOI-2	836.43	29	SST-2	836.86
4	MEI-3	836.52	17	SOI-3	835.01	30	SST-3	836.89
5	MEI-4	836.28	18	SOI-4	836.61	31	SST-4	836.41
6	MEI-5	834.67	19	SOI-5	834.39	32	SST-5	835.47
7	MEI-6	833.75	20	SOI-6	833.34	33	SST-6	834.25
8	MEI-7	831.65	21	SOI-7	834.50	34	SST-7	833.49
9	MEI-8	829.73	22	SOI-8	830.10	35	SST-8	830.70
10	MEI-9	827.54	23	SOI-9	828.39	36	SST-9	827.63
11	MEI-10	826.68	24	SOI-10	832.30	37	SST-10	827.59
12	MEI-11	827.57	25	SOI-11	829.76	38	SST-11	828.30
13	MEI-12	830.71	26	SOI-12	831.76	39	SST-12	828.46

5.1.5. Quality of fitted non-stationary model

The probability–probability (PP) plots and quantile–quantile (QQ) plots can be used to check the quality of a fitted model (Coles, 2001; Katz et al., 2002; Sugahara et al., 2009). Let the values $Y = y_1, y_2 \ldots, y_n$ are the n excesses of a threshold u and it is fitted with non-stationary GP distribution. As the n exceedances are not identically distributed, they have to be transformed to residuals (ε) (exponential distribution with unit scale parameter) for obtaining the PP and QQ plots (Katz et al., 2002; Katz, 2013).

$$\varepsilon_i = \frac{1}{\hat{\xi}} \log\left(1 + \frac{\hat{\xi}}{\hat{\sigma}} y_i\right) \tag{7}$$

where $\hat{\xi}$ and $\hat{\sigma}$ are estimated shape and scale parameter of the distribution. If $\hat{\varepsilon}$ is the ordered values of ε, then the PP plot points (Katz et al., 2002) are given by Eq. (8) and the QQ plot points (Katz et al., 2002) are given by Eq. (9).

$$\left(\frac{i}{n+1}, 1 - \exp(-\hat{\varepsilon})\right) \tag{8}$$

$$\left(-\log\left(1 - \frac{i}{n+1}\right), \hat{\varepsilon}\right) \tag{9}$$

5.2. Modelling non-stationarity in frequency of extreme rainfall

The frequency of extreme rainfall (i.e. the rate at which the threshold is exceeded), can be approximated by a one dimensional Poisson process with rate parameter $\lambda > 0$ (Katz, 2013). Specifically, the number of exceedance ($N(T)$) of threshold (u) within a time period (T) is approximately Poisson distribution with mean λT (Katz, 2013). Further, The Generalized Linear Model (GLM) framework is used to incorporate trend in rate parameter λ and Eq. (11) gives the non-stationary Poisson rate parameter.

$$E[N(T)] = \lambda T \tag{10}$$

$$\lambda(i) = \exp(\lambda_0 + \lambda_1 c_1 + \lambda_2 c_2 + \lambda_3 c_3 + \lambda_4 c_4) \tag{11}$$

The slope parameters λ_1, λ_2, λ_3 and λ_4 represent the trend due to the effect of physical covariates c_1, c_2, c_3 and c_4 respectively. Apart from stationary model, based on four covariates and their combinations, fifteen non-stationary models are constructed (refer Table 5). For stationary model, the values of c_1, c_2, c_3 and c_4 are zero. The parameters are estimated by the method of maximum likelihood and AICc is used to select the best model. The physical covariate(s) of the best Poisson model is/are the most significant physical process/processes which is/are responsible for the change in frequency of extreme rainfall. The list of GPD and Poisson models constructed to model non-stationarity in the intensity and frequency of extreme rainfall of Hyderabad city and their specifications are listed in Table 5. The R programming language and R packages "ismev", "stats" and "extRemes" are used to model the non-stationarity.

5.3. Monsoon months

5.3.1. Daily extreme rainfall

The MRL estimated extreme daily rainfall value for monsoon months is 38.57 mm and it is the 95th percentile rainfall of the period. Between 1971 and 2013, during the monsoon months, the number of rainfall events which has intensity more than 38.57 mm/day is 106 and after declustering the number of events is reduced to 99. As MEI, SOI and SST are used as ENSO indicators with lag up to 12 months, the best ENSO index with best lag which represents the non-stationarity in monsoon rainfall need to be identified first. Thus, the non-stationary GPD models are constructed for monsoon months' daily rainfall POT series with different ENSO indices with different lag as covariate. The best ENSO index with best lag is identified based on AICc value. Table 7 shows the non-stationary GPD models' performance for monsoon months' daily extreme rainfall with different ENSO indices as covariates. The ENSO index MEI with lag 10 months is chosen as the best ENSO index for monsoon months. Thus, the MEI with lag 10 months is used for further modelling of non-stationarity in intensity and frequency of daily and 4-h extreme rainfall of monsoon months. With chosen ENSO index (i.e. MEI-10), the GPD and Poisson models (refer Table 5) are constructed based on four physical covariates and their combinations.

The different GPD model's performance for monsoon months' daily extreme rainfall with different physical covariates and their combinations are given in Table 8. Among 16 GPD models the GPD-11 is found to be the best model for monsoon months' daily extreme rainfall intensity. It is worth to note that the stationary model (GPD-1) is ranked 12 and it is not even considerable model based on Δ_i value (Burnham and Anderson, 2004). The PP plot and QQ plot can be used to check the quality of a fitted model, however, the PP plot is less helpful than the QQ plot for discerning differences in the quality of fitting (Sugahara et al., 2009). For brevity, the QQ plots of GPD-1 (stationary) and GPD-11 (best model) are shown in Fig.13(a) and (b) respectively. The QQ plots clearly show the superiority of GPD-11 against GPD-1.

The different Poisson model's performance for monsoon months' daily extreme rainfall frequency with different physical covariates and their combinations are listed in Table 9. Among 16 Poisson models the P-2 is found to be the best model based on Δ_i and the stationary model P-1 is ranked 6.

5.3.2. Monsoon months' 1 a.m. to 4 a.m. extreme rainfall

12.083 mm/4-h is the MRL plot interpreted extreme rainfall value for 1 a.m. to 4 a.m. monsoon rainfall and it is the 91th

Table 8
GPD models' performance with **monsoon daily** extreme rainfall. Models are sorted according to Δ_i value.

Rank	Model ID	σ_0 (SE)	σ_1 (SE)	σ_2 (SE)	σ_3 (SE)	σ_4 (SE)	ξ (SE)	AICc	Δ_i
1	GPD-11	2.917 (0.240)	0.753 (0.532)	−0.319 (0.097)			0.086 (0.124)	826.65	0.00
2	GPD-5	3.17 (0.167)	−0.330 (0.092)				0.042 (0.130)	826.68	0.03
3	GPD-8	1.798 (1.064)	0.247 (0.189)	−0.293 (0.100)			0.083 (0.127)	827.00	0.35
4	GPD-10	3.148 (0.172)	−0.021 (0.036)	−0.329 (0.091)			0.020 (0.136)	828.51	1.85
5	GPD-15	2.918 (0.241)	−0.007 (0.04)	0.724 (0.556)	−0.319 (0.096)		0.079 (0.131)	828.84	2.19
6	GPD-14	2.775 (1.926)	0.030 (0.405)	0.683 (1.139)	−0.316 (0.107)		0.087 (0.125)	828.87	2.21
7	GPD-13	1.838 (1.122)	0.239 (0.202)	−0.004 (0.041)	−0.294 (0.100)		0.078 (0.135)	829.21	2.56
8	GPD-2	0.816 (1.046)	0.406 (0.191)				0.197 (0.125)	832.32	5.67
9	GPD-4	2.708 (0.231)	0.990 (0.564)				0.213 (0.126)	833.76	7.10
10	GPD-7	0.454 (1.851)	0.488 (0.396)	−0.279 (1.161)			0.192 (0.127)	834.44	7.78
11	GPD-6	0.787 (1.077)	0.412 (0.20)	0.004 (0.043)			0.199 (0.128)	834.49	7.83
12	GPD-1	19.821 (3.276)					0.209 (0.133)	834.79	8.14
13	GPD-9	2.707 (0.232)	−0.003 (0.043)	0.98 (0.581)			0.211 (0.129)	835.92	9.27
14	GPD-12	0.408 (1.873)	0.499 (0.402)	0.005 (0.043)	−0.293 (1.161)		0.194 (0.129)	836.64	9.99
15	GPD-3	2.964 (0.173)	−0.019 (0.041)				0.193 (0.135)	836.71	10.06
16	GPD-16	7.911 (2.202)	−1.117 (0.472)	−0.007 (0.043)	4.265 (1.375)	−0.415 (0.116)	0.186 (0.139)	840.04	13.39

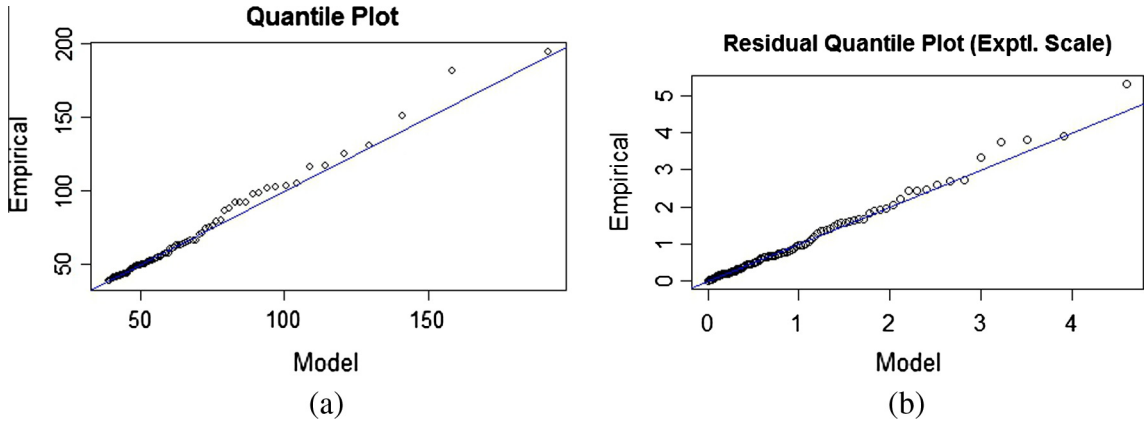

Fig. 13. The QQ plots of (a) GPD-1, (b) GPD-11 from monsoon months' daily extreme rainfall.

Table 9
Poisson models' performance with **monsoon daily** extreme rainfall. Models are sorted according to Δ_i value.

Rank	Model ID	λ_0 (SE)	λ_1 (SE)	λ_2 (SE)	λ_3 (SE)	λ_4 (SE)	AICc	Δ_i
1	P-2	−5.233 (0.801)	0.295 (0.149)				927.76	0.00
2	P-4	−3.886 (0.155)	0.838 (0.454)				928.26	0.50
3	P-8	−5.319 (0.817)	0.308 (0.152)	0.103 (0.096)			928.62	0.85
4	P-11	−3.889 (0.156)	0.805 (0.458)	0.073 (0.095)			929.68	1.92
5	P-7	−4.922 (1.388)	0.224 (0.298)	0.248 (0.908)			929.69	1.93
6	P-1	−3.685 (0.101)					929.70	1.94
7	P-6	−5.238 (0.806)	0.296 (0.152)	0.002 (0.031)			929.76	2.00
8	P-9	−3.890 (0.162)	−0.003 (0.031)	0.833 (0.458)			930.26	2.50
9	P-13	−5.310 (0.822)	0.305 (0.155)	−0.003 (0.031)	0.105 (0.097)		930.61	2.85
10	P-14	−5.383 (1.473)	0.322 (0.315)	−0.050 (0.955)	0.105 (0.101)		930.62	2.85
11	P-5	−3.700 (0.102)	0.091 (0.095)				930.78	3.01
12	P-3	−3.705 (0.118)	−0.010 (0.031)				931.60	3.83
13	P-15	−3.900 (0.163)	−0.007 (0.031)	0.789 (0.464)	0.077 (0.097)		931.63	3.87
14	P-12	−4.929 (1.401)	0.226 (0.302)	0.001 (0.031)	0.246 (0.911)		931.69	3.93
15	P-10	−3.730 (0.121)	−0.015 (0.031)	0.099 (0.096)			932.54	4.78
16	P-16	−5.368 (1.480)	0.318 (0.318)	−0.003 (0.031)	−0.045 (0.955)	0.106 (0.101)	932.61	4.85

percentile rainfall of the period. Total 74 rainfall events are identified as extreme rainfall events in this period and after declustering the number of extreme events count is 60. The 16 GPD models fitted with these extreme rainfall events are given in Table 10 and the GPD-2 is found to be the best model for monsoon months' 1 a.m. to 4 a.m. extreme rainfall intensity.

Further, it is noted that the GPD-1 model is ranked 8 and it is not even considerable based on Δ_i value. The QQ plots of GPD-1 (stationary) and GPD-2 (best model) are shown in Fig. 14 (a) and (b) respectively. Table 11 reveals the different Poisson model's performance for monsoon months' 1 a.m. to 4 a.m. extreme rainfall frequency with different physical covariates and their combinations. Among 16 Poisson models, the stationary model P-1 itself found to be the best model for monsoon months' 1 a.m. to 4 a.m. extreme rainfall frequency.

5.3.3. Monsoon months' 5 p.m. to 8 p.m. extreme rainfall

The MRL estimated extreme rainfall value for 5 p.m. to 8 a.m. monsoon rainfall is 17 mm and it is the 94th percentile rainfall of the period. Total 66 rainfall events are identified as extreme

Table 10
GPD models' performance with **monsoon 1 a.m. to 4 a.m.** extreme rainfall. Models are sorted according to Δ_i value.

Rank	Model ID	σ_0 (SE)	σ_1 (SE)	σ_2 (SE)	σ_3 (SE)	σ_4 (SE)	ξ (SE)	AICc	Δ_i
1	GPD-2	0.239 (1.022)	0.514 (0.191)				−0.014 (0.153)	477.48	0.00
2	GPD-7	−0.811 (1.546)	0.762 (0.331)	−0.926 (1.040)			−0.048 (0.173)	479.04	1.56
3	GPD-8	0.323 (1.061)	0.501 (0.195)	−0.032 (0.110)			−0.024 (0.159)	479.70	2.22
4	GPD-6	0.229 (1.023)	0.518 (0.193)	0.007 (0.043)			−0.011 (0.153)	479.75	2.27
5	GPD-4	2.62 (0.249)	1.095 (0.640)				0.073 (0.145)	480.92	3.44
6	GPD-12	−0.819 (1.549)	0.765 (0.332)	0.006 (0.043)	−0.921 (1.041)		−0.044 (0.173)	481.40	3.92
7	GPD-14	−0.845 (1.747)	0.769 (0.372)	−0.949 (1.136)	0.005 (0.115)		−0.048 (0.173)	481.42	3.94
8	GPD-1	17.311 (3.654)					0.126 (0.168)	481.48	4.00
9	GPD-13	0.300 (1.063)	0.507 (0.198)	0.006 (0.043)	−0.030 (0.110)		−0.019 (0.160)	482.06	4.58
10	GPD-11	2.672 (0.261)	1.089 (0.621)	−0.088 (0.118)			0.029 (0.156)	482.73	5.25
11	GPD-9	2.628 (0.255)	0.006 (0.047)	1.095 (0.642)			0.076 (0.147)	483.21	5.73
12	GPD-5	2.896 (0.228)	−0.073 (0.124)				0.089 (0.182)	483.38	5.90
13	GPD-3	2.859 (0.219)	0.007 (0.051)				0.132 (0.173)	483.68	6.20
14	GPD-15	2.672 (0.264)	0.002 (0.045)	1.091 (0.627)	−0.085 (0.120)		0.035 (0.162)	485.11	7.63
15	GPD-10	2.896 (0.230)	0.001 (0.051)	−0.073 (0.128)			0.090 (0.195)	485.68	8.20
16	GPD-16	−12.451 (7.930)	3.240 (1.695)	0.098 (0.093)	−9.624 (5.552)	0.161 (0.231)	1.331 (0.987)	512.58	35.10

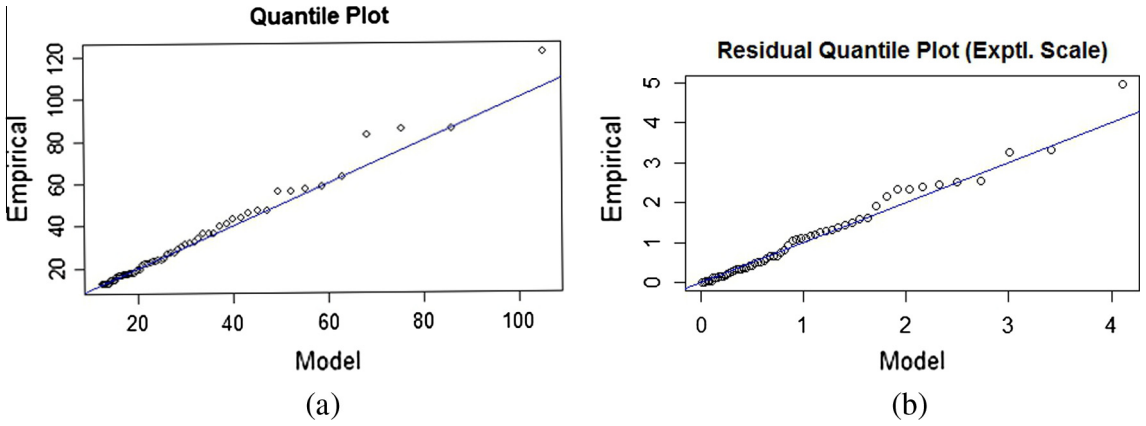

Fig. 14. The QQ plots of (a) GPD-1, (b) GPD-2 from monsoon 1 a.m. to 4 a.m. extreme rainfall.

Table 11
Poisson models' performance with **monsoon 1 a.m. to 4 a.m.** extreme rainfall. Models sorted according to Δ_i value.

Rank	Model ID	λ_0 (SE)	λ_1 (SE)	λ_2 (SE)	λ_3 (SE)	λ_4 (SE)	AICc	Δ_i
1	P-1	−4.189 (0.129)					624.64	0.00
2	P-2	−4.942 (1.007)	0.144 (0.190)				626.06	1.42
3	P-4	−4.284 (0.189)	0.415 (0.580)				626.13	1.49
4	P-3	−4.222 (0.153)	−0.017 (0.040)				626.46	1.82
5	P-5	−4.193 (0.130)	0.034 (0.123)				626.57	1.93
6	P-8	−4.962 (1.015)	0.147 (0.191)	0.038 (0.123)			627.97	3.33
7	P-6	−4.910 (1.013)	0.134 (0.194)	−0.011 (0.040)			627.99	3.35
8	P-9	−4.304 (0.150)	−0.013 (0.040)	0.390 (0.583)			628.02	3.38
9	P-7	−4.770 (1.768)	0.105 (0.380)	0.137 (1.161)			628.05	3.41
10	P-11	−4.284 (0.190)	0.403 (0.584)	0.024 (0.124)			628.09	3.45
11	P-10	−4.232 (0.156)	−0.019 (0.040)	0.044 (0.124)			628.34	3.70
12	P-13	−4.926 (1.021)	0.135 (0.195)	−0.014 (0.041)	0.044 (0.124)		629.87	5.23
13	P-15	−4.307 (0.201)	−0.015 (0.040)	0.369 (0.590)	0.033 (0.125)		629.95	5.31
14	P-12	−4.700 (1.778)	0.086 (0.385)	−0.012 (0.040)	0.166 (1.159)		629.97	5.33
15	P-14	−4.918 (1.850)	0.137 (0.398)	0.035 (1.218)	0.037 (0.129)		629.98	5.34
16	P-16	−4.856 (1.850)	0.119 (0.399)	−0.014 (0.041)	0.055 (1.209)	0.042 (0.130)	631.87	7.23

rainfall events in this period and after declustering the number of extreme events count is 58. Table 12 shows the performances of 16 GPD model fitted with monsoon months' 5 p.m. to 8 p.m. extreme rainfall events. For monsoon months' 5 p.m. to 8 p.m. extreme rainfall intensity, the non-stationary model GPD-5 is found to be the best model. In addition, it is noted that the model GPD-1 is ranked 9 and it is not even considerable based on Δ_i value and the superiority of GPD-5 against GPD-1 can be observed from Fig. 15(a) and (b). The different Poisson model's performance for monsoon months' 5 p.m. to 8 p.m. extreme rainfall frequency with different physical covariates and their combinations are given in Table 13. In the monsoon months' 5 p.m. to 8 p.m. extreme rainfall frequency, the P-1 is found to be the best model based on Δ_i value.

5.3.4. Monsoon months' 9 p.m. to 12 a.m. extreme rainfall

16.856 mm/4-h is the MRL estimated extreme rainfall value for 9 p.m. to 12 a.m. monsoon rainfall and it is the 92nd percentile rainfall of the period. Total 77 rainfall events are identified as

Table 12
GPD models' performance with **monsoon 5 p.m. to 8 p.m.** extreme rainfall. Models are sorted according to Δ_i value.

Rank	Model ID	σ_0 (SE)	σ_1 (SE)	σ_2 (SE)	σ_3 (SE)	σ_4 (SE)	ξ (SE)	AICc	Δ_i
1	GPD-5	3.015 (0.194)	−0.259 (0.086)				−0.321 (0.146)	431.43	0.00
2	GPD-8	2.000 (0.940)	0.182 (0.158)	−0.288 (0.102)			−0.271 (0.168)	431.90	0.47
3	GPD-11	2.822 (0.294)	0.532 (0.495)	−0.307 (0.104)			−0.259 (0.176)	432.06	0.62
4	GPD-10	2.971 (0.211)	−0.033 (0.029)	−0.269 (0.088)			−0.350 (0.150)	432.33	0.90
5	GPD-13	2.242 (1.172)	0.135 (0.211)	−0.014 (0.043)	−0.287 (0.101)		−0.291 (0.181)	434.21	2.78
6	GPD-14	1.934 (2.261)	0.198 (0.499)	−0.052 (1.547)	−0.286 (0.118)		−0.273 (0.181)	434.30	2.87
7	GPD-15	2.858 (0.303)	−0.017 (0.042)	0.356 (0.629)	−0.298 (0.105)		−0.288 (0.191)	434.31	2.88
8	GPD-2	1.205 (1.201)	0.296 (0.214)				−0.053 (0.125)	435.22	3.79
9	GPD-1	17.457 (3.209)					−0.143 (0.129)	435.32	3.89
10	GPD-3	2.770 (0.187)	−0.047 (0.038)				−0.156 (0.108)	435.97	4.54
11	GPD-4	2.599 (0.300)	0.691 (0.681)				−0.052 (0.140)	436.27	4.84
12	GPD-16	2.144 (2.272)	0.158 (0.496)	−0.014 (0.043)	−0.081 (1.483)	−0.283 (0.117)	−0.296 (0.193)	436.70	5.27
13	GPD-7	−0.554 (2.221)	0.716 (0.500)	−1.536 (1.659)			−0.140 (0.171)	436.76	5.32
14	GPD-6	1.463 (1.472)	0.244 (0.275)	−0.016 (0.053)			−0.068 (0.135)	437.44	6.01
15	GPD-9	2.666 (0.333)	−0.035 (0.052)	0.322 (0.877)			−0.103 (0.171)	438.14	6.71
16	GPD-12	−0.242 (2.333)	0.655 (0.516)	−0.018 (0.051)	−1.549 (1.600)		−0.163 (0.189)	439.03	7.60

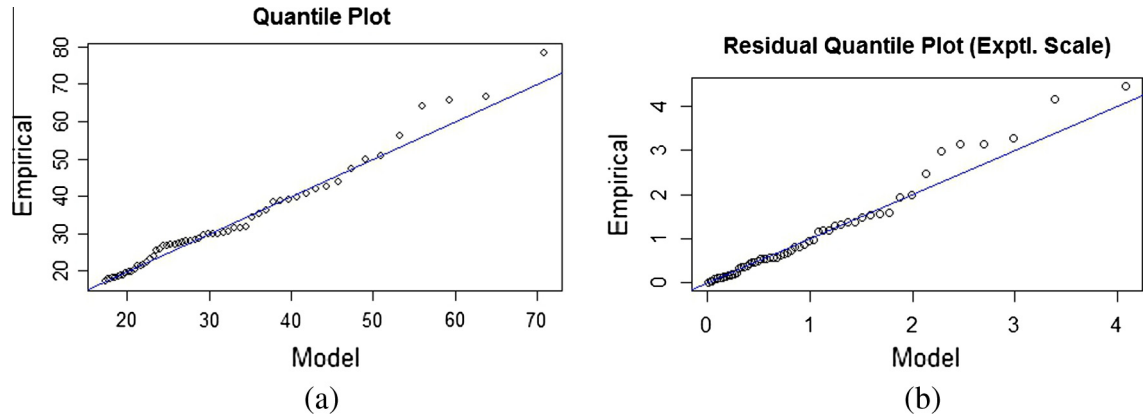

Fig. 15. The QQ plots of (a) GPD-1, (b) GPD-2 from monsoon 5 p.m. to 8 p.m. extreme rainfall.

Table 13
Poisson models' performance with **monsoon 5 p.m. to 8 p.m.** extreme rainfall. Models are sorted according to Δ_i value.

Rank	Model ID	λ_0 (SE)	λ_1 (SE)	λ_2 (SE)	λ_3 (SE)	λ_4 (SE)	AICc	Δ_i
1	P-1	−4.223 (0.131)					607.82	0.00
2	P-4	−4.273 (0.188)	0.223 (0.589)				609.67	1.86
3	P-2	−4.584 (1.016)	0.069 (0.193)				609.69	1.87
4	P-3	−4.216 (0.151)	0.003 (0.040)				609.81	2.00
5	P-5	−4.224 (0.132)	0.009 (0.125)				609.81	2.00
6	P-9	−4.265 (0.197)	0.005 (0.040)	0.233 (0.594)			611.66	3.84
7	P-6	−4.602 (1.023)	0.075 (0.197)	0.006 (0.041)			611.67	3.85
8	P-7	−4.384 (1.786)	0.024 (0.385)	0.159 (1.175)			611.67	3.86
9	P-11	−4.272 (0.188)	0.221 (0.593)	0.004 (0.126)			611.68	3.86
10	P-8	−4.588 (1.018)	0.070 (0.193)	0.011 (0.126)			611.68	3.87
11	P-10	−4.218 (0.154)	0.003 (0.041)	0.008 (0.128)			611.81	3.99
12	P-12	−4.420 (1.807)	0.034 (0.392)	0.006 (0.041)	0.144 (1.183)		613.66	5.84
13	P-15	−4.265 (0.198)	0.005 (0.041)	0.232 (0.600)	0.000 (0.129)		613.67	5.85
14	P-13	−4.604 (1.025)	0.075 (0.197)	0.006 (0.041)	0.008 (0.128)		613.67	5.85
15	P-14	−4.409 (1.859)	0.030 (0.401)	0.142 (1.230)	0.006 (0.132)		613.68	5.86
16	P-16	−4.433 (1.871)	0.037 (0.405)	0.006 (0.041)	0.135 (1.236)	0.003 (0.134)	615.66	7.85

extreme rainfall events in this period and after declustering the number of extreme events count is reduced to 66. The 16 GPD models fitted with these extreme rainfall events are given in Table 14. The GPD-2 is found to be the best model for monsoon months' 9 p.m. to 12 a.m. extreme rainfall intensity. Further, it is noted that the GPD-1 model is ranked 11 and it is not even considerable based on Δ_i value. The QQ plots of GPD-1 (stationary) and GPD-2 (best model) are shown in Fig. 16(a) and (b) respectively. The QQ plots clearly show the superiority of GPD-2 against GPD-1.

Table 15 reveals the different Poisson model's performance for monsoon months' 9 p.m. to 12 a.m. extreme rainfall frequency. The P-5 is found to be the best model for monsoon months' 9 p.m. to 12 a.m. extreme rainfall frequency. It is worth to note that the model P-1 is not even considerable and it is ranked 5 among 16.

5.4. Non-monsoon months

5.4.1. Daily extreme rainfall

The MRL estimated extreme rainfall value for daily non-monsoon rainfall is 38.49 mm and it is the 95th percentile rainfall of the period. Between 1971 and 2013, during non-monsoon months, the number of rainfall events which has intensity more

Table 14
GPD models' performance with **monsoon 9 p.m. to 12 a.m.** extreme rainfall. Models are sorted according to Δ_i value.

Rank	Model ID	σ_0 (SE)	σ_1 (SE)	σ_2 (SE)	σ_3 (SE)	σ_4 (SE)	ξ (SE)	AICc	Δ_i
1	GPD-2	0.629 (0.876)	0.412 (0.161)				−0.261 (0.115)	467.05	0.00
2	GPD-4	2.513 (0.195)	1.146 (0.484)				−0.263 (0.107)	468.13	1.08
3	GPD-8	0.459 (0.964)	0.435 (0.172)	0.054 (0.127)			−0.234 (0.129)	469.13	2.09
4	GPD-6	0.673 (0.903)	0.400 (0.167)	−0.007 (0.027)			−0.254 (0.121)	469.24	2.19
5	GPD-7	0.952 (1.481)	0.339 (0.315)	0.253 (0.959)			−0.265 (0.115)	469.25	2.20
6	GPD-9	2.470 (0.216)	−0.025 (0.024)	1.177 (0.481)			−0.274 (0.117)	469.35	2.30
7	GPD-11	2.492 (0.248)	1.162 (0.503)	0.017 (0.127)			−0.252 (0.133)	470.38	3.33
8	GPD-13	0.494 (0.981)	0.421 (0.176)	−0.011 (0.029)	0.066 (0.131)		−0.222 (0.132)	471.32	4.27
9	GPD-12	1.448 (1.833)	0.224 (0.399)	−0.015 (0.031)	0.563 (1.181)		−0.261 (0.121)	471.36	4.31
10	GPD-15	2.419 (0.259)	−0.028 (0.026)	1.215 (0.503)	0.042 (0.127)		−0.253 (0.129)	471.58	4.54
11	GPD-1	15.951 (2.746)					−0.227 (0.124)	471.74	4.70
12	GPD-3	2.739 (0.186)	−0.016 (0.026)				−0.226 (0.129)	473.55	6.50
13	GPD-16	1.159 (1.956)	0.272 (0.418)	−0.017 (0.032)	0.484 (1.221)	0.058 (0.131)	−0.23 (0.134)	473.58	6.54
14	GPD-5	2.748 (0.212)	0.022 (0.129)				−0.214 (0.143)	473.91	6.86
15	GPD-10	2.701 (0.220)	−0.019 (0.028)	0.039 (0.129)			−0.208 (0.139)	475.72	8.67
16	GPD-14	6.641 (2.244)	−0.918 (0.489)	3.790 (1.401)	0.056 (0.126)		−0.144 (0.147)	484.77	17.73

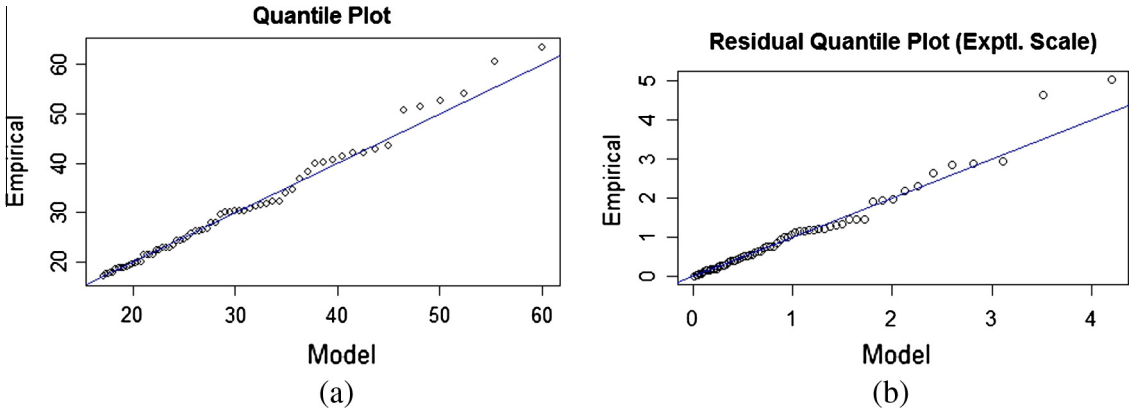

Fig. 16. The QQ plots of (a) GPD-1, (b) GPD-2 from monsoon 9 p.m. to 12 p.m. extreme rainfall.

Table 15
Poisson models' performance with **monsoon 9 p.m. to 12 a.m.** extreme rainfall. Models are sorted according to Δ_i value.

Rank	Model ID	λ_0 (SE)	λ_1 (SE)	λ_2 (SE)	λ_3 (SE)	λ_4 (SE)	AICc	Δ_i
1	P-5	−4.157 (0.131)	0.255 (0.114)				671.41	0.00
2	P-10	−4.127 (0.146)	0.016 (0.037)	0.248 (0.116)			673.23	1.82
3	P-11	−4.114 (0.176)	−0.201 (0.573)	0.260 (0.115)			673.29	1.88
4	P-8	−3.847 (0.978)	−0.060 (0.188)	0.253 (0.114)			673.31	1.90
5	P-1	−4.093 (0.123)					674.32	2.91
6	P-15	−4.094 (0.183)	0.014 (0.037)	−0.171 (0.579)	0.253 (0.117)		675.15	3.74
7	P-13	−3.898 (0.987)	−0.045 (0.192)	0.014 (0.038)	0.247 (0.115)		675.18	3.77
8	P-14	−4.065 (1.751)	−0.011 (0.377)	−0.172 (1.149)	0.259 (0.121)		675.30	3.88
9	P-3	−4.042 (0.136)	0.029 (0.037)				675.71	4.30
10	P-2	−3.732 (0.941)	−0.060 (0.181)				676.17	4.76
11	P-4	−4.086 (0.171)	−0.036 (0.551)				676.32	4.91
12	P-16	−4.170 (1.785)	0.017 (0.386)	0.015 (0.038)	−0.214 (1.165)	0.255 (0.122)	677.15	5.74
13	P-6	−3.813 (0.949)	−0.045 (0.185)	0.027 (0.038)	0.000 (0.129)		677.65	6.24
14	P-9	−4.046 (0.178)	0.029 (0.037)	0.015 (0.558)			677.71	6.30
15	P-7	−3.009 (1.632)	−0.234 (0.354)	0.581 (1.079)			677.89	6.48
16	P-12	3.160 (1.662)	−0.194 (0.362)	0.026 (0.038)	0.522 (1.097)		679.43	8.02

than 38.49 is 88 and after declustering the number of events is reduced to 79. Similar to monsoon months, first the best ENSO index with best lag is identified for non-monsoon months. Table 16 shows the non-stationary GPD models' performance for non-monsoon months' daily extreme rainfall with different ENSO indices as covariate. The ENSO index SOI with lag 11 months is chosen as the best ENSO index for non-monsoon months. Thus, the SOI with lag 11 months is used for further modelling of non-stationarity in intensity and frequency of daily and 4-h extreme rainfall of non-monsoon months.

Table 17 reveals the different GPD model's performance for non-monsoon months' daily extreme rainfall with different physical covariates and their combinations. Among 16 GPD models the GPD-5 is found to be the best model for non-monsoon months' daily extreme rainfall intensity. In addition, it is worth to note that the stationary model (GPD-1) model is ranked 9 and it is not even

Table 16
Non-stationary GPD models' performance for **non-monsoon daily** extreme rainfall with different ENSO indices as covariate.

S. no.	MEI	AICc	S. no.	SOI	AICc	S. no.	SST	AICc
1	MEI-0	635.66	14	SOI-0	635.44	27	SST-0	635.94
2	MEI-1	635.50	15	SOI-1	635.00	28	SST-1	635.80
3	MEI-2	635.71	16	SOI-2	635.88	29	SST-2	635.88
4	MEI-3	635.80	17	SOI-3	635.93	30	SST-3	635.77
5	MEI-4	635.94	18	SOI-4	635.90	31	SST-4	635.92
6	MEI-5	635.81	19	SOI-5	635.91	32	SST-5	635.84
7	MEI-6	635.84	20	SOI-6	634.67	33	SST-6	635.44
8	MEI-7	635.96	21	SOI-7	635.58	34	SST-7	635.96
9	MEI-8	635.73	22	SOI-8	635.96	35	SST-8	635.56
10	MEI-9	635.79	23	SOI-9	635.96	36	SST-9	635.11
11	MEI-10	635.02	24	SOI-10	635.94	37	SST-10	635.05
12	MEI-11	635.18	25	SOI-11	629.82	38	SST-11	635.26
13	MEI-12	635.82	26	SOI-12	635.09	39	SST-12	635.76

Table 17
GPD models' performance with **non-monsoon daily** extreme rainfall. Models are sorted according to Δ_i value.

Rank	Model ID	σ_0 (SE)	σ_1 (SE)	σ_2 (SE)	σ_3 (SE)	σ_4 (SE)	ξ (SE)	AICc	Δ_i
1	GPD-5	3.018 (0.164)	−0.165 (0.068)				0.022 (0.121)	629.82	0
2	GPD-10	2.869 (0.205)	−0.048 (0.039)	−0.163 (0.069)			0.014 (0.111)	630.58	0.76
3	GPD-8	3.856 (0.839)	−0.165 (0.164)	−0.162 (0.068)			0.016 (0.122)	631.03	1.21
4	GPD-11	3.047 (0.182)	−0.155 (0.402)	−0.164 (0.068)			0.018 (0.123)	631.89	2.07
5	GPD-13	3.689 (0.872)	−0.164 (0.170)	−0.049 (0.041)	−0.159 (0.069)		0.023 (0.115)	631.98	2.17
6	GPD-14	4.795 (1.441)	−0.373 (0.308)	0.613 (0.769)	−0.165 (0.067)		0.024 (0.119)	632.64	2.82
7	GPD-15	2.889 (0.222)	−0.047 (0.040)	−0.090 (0.413)	−0.163 (0.069)		0.013 (0.111)	632.81	2.99
8	GPD-16	4.849 (1.478)	−0.426 (0.319)	−0.054 (0.041)	0.804 (0.806)	−0.164 (0.069)	0.027 (0.111)	633.29	3.47
9	GPD-1	19.44 (3.182)					0.018 (0.119)	633.80	3.98
10	GPD-3	2.788 (0.209)	−0.055 (0.040)				0.014 (0.109)	634.07	4.25
11	GPD-2	3.941 (0.856)	−0.190 (0.166)				0.005 (0.121)	634.68	4.86
12	GPD-6	3.698 (0.894)	−0.181 (0.174)	−0.054 (0.042)			0.021 (0.113)	635.20	5.38
13	GPD-4	3.017 (0.186)	−0.231 (0.414)				0.008 (0.122)	635.66	5.84
14	GPD-9	2.817 (0.230)	−0.054 (0.041)	−0.147 (0.433)			0.015 (0.110)	636.17	6.36
15	GPD-7	4.621 (1.409)	−0.343 (0.302)	0.466 (0.758)			0.017 (0.122)	636.50	6.68
16	GPD-12	4.692 (1.465)	−0.407 (0.317)	−0.061 (0.042)	0.695 (0.804)		0.028 (0.112)	636.69	6.88

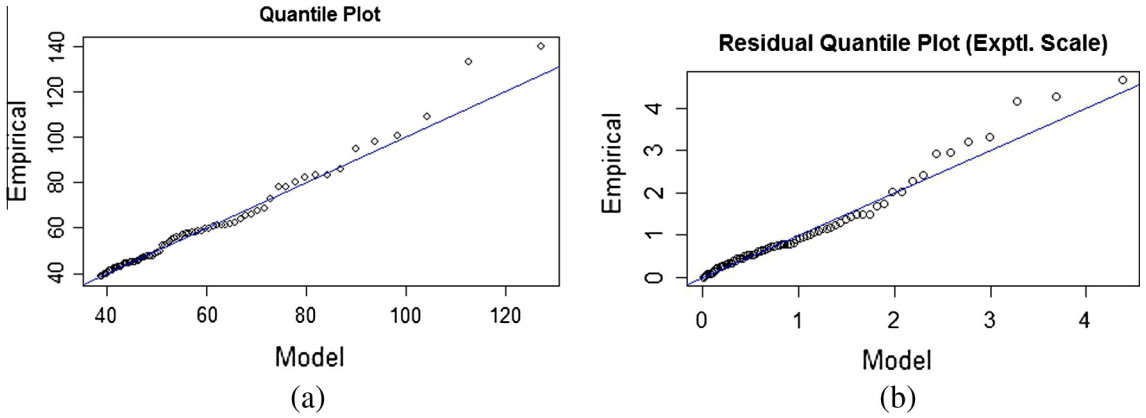

Fig. 17. The QQ plots of (a) GPD-1, (b) GPD-5 from non-monsoon daily extreme rainfall.

considerable model based on Δ_i value. The superiority of GPD-5 against GPD-1 can be observed from QQ plots shown in Fig. 17 (a) and (b). Table 18 provides the different Poisson model's performance with different physical covariates and their combinations for non-monsoon months' daily extreme rainfall frequency. Based on Poisson models' performances, the non-stationary model P-9 is found to be the best model for non-monsoon months' daily extreme rainfall frequency. The stationary model P-1 is ranked 10 and it is not even considerable based on Δ_i value.

5.4.2. Non-monsoon months' 5 p.m. to 8 p.m. extreme rainfall

16.4 mm/4-h is the MRL estimated extreme rainfall value for 5 p.m. to 8 p.m. non-monsoon rainfall and it is the 90th percentile rainfall of the period. Total 76 rainfall events are identified as extreme

Table 18
Poisson models' performance with **non-monsoon daily** extreme rainfall. Models are sorted according to Δ_i value.

Rank	Model ID	λ_0 (SE)	λ_1 (SE)	λ_2 (SE)	λ_3 (SE)	λ_4 (SE)	AICc	Δ_i
1	P-9	−5.074 (0.173)	−0.082 (0.034)	−0.663 (0.420)			944.54	0.00
2	P-3	−5.214 (0.154)	−0.084 (0.034)				945.00	0.46
3	P-6	−4.118 (0.844)	−0.214 (0.163)	−0.085 (0.034)			945.28	0.74
4	P-15	−5.089 (0.174)	−0.080 (0.034)	−0.647 (0.417)	0.038 (0.054)		946.03	1.49
5	P-10	−5.228 (0.155)	−0.082 (0.034)	0.041 (0.054)			946.42	1.88
6	P-12	−4.979 (1.307)	−0.020 (0.277)	−0.082 (0.034)	−0.620 (0.721)		946.53	1.99
7	P-13	−4.154 (0.837)	−0.209 (0.162)	−0.083 (0.034)	0.040 (0.054)		946.74	2.20
8	P-16	−4.994 (1.304)	−0.020 (0.276)	−0.080 (0.034)	−0.603 (0.719)	0.038 (0.054)	948.03	3.49
9	P-4	−4.856 (0.137)	−0.710 (0.433)				949.43	4.89
10	P-1	−5.001 (0.113)					950.10	5.56
11	P-11	−4.884 (0.141)	−0.687 (0.427)	0.053 (0.056)			950.54	6.00
12	P-2	−3.981 (0.854)	−0.198 (0.166)				950.67	6.13
13	P-5	−5.026 (0.117)	0.056 (0.057)				951.12	6.58
14	P-7	−5.105 (1.315)	0.053 (0.278)	−0.822 (0.733)			951.39	6.85
15	P-8	−4.023 (0.843)	−0.195 (0.164)	0.056 (0.057)			951.69	7.15
16	P-14	−5.105 (1.310)	0.047 (0.277)	−0.787 (0.731)	0.052 (0.056)		952.51	7.97

Table 19
GPD models' performance with **non-monsoon 5 p.m. to 8 p.m.** extreme rainfall. Models are sorted according to Δ_i value.

Rank	Model ID	σ_0 (SE)	σ_1 (SE)	σ_2 (SE)	σ_3 (SE)	σ_4 (SE)	ξ (SE)	AICc	Δ_i
1	GPD-4	2.917 (0.190)	−0.799 (0.479)				−0.077 (0.114)	558.58	0.00
2	GPD-1	15.378 (2.729)					−0.079 (0.136)	559.52	0.94
3	GPD-2	3.749 (0.822)	−0.199 (0.160)				−0.052 (0.121)	559.99	1.41
4	GPD-9	2.986 (0.209)	0.031 (0.035)	−0.822 (0.475)			−0.057 (0.117)	560.01	1.43
5	GPD-11	2.919 (0.191)	−0.824 (0.491)	0.016 (0.062)			−0.074 (0.116)	560.75	2.17
6	GPD-7	2.866 (1.025)	0.011 (0.219)	−0.830 (0.678)			−0.076 (0.118)	560.81	2.23
7	GPD-3	2.776 (0.186)	0.026 (0.035)				−0.053 (0.141)	561.10	2.52
8	GPD-6	3.802 (0.828)	−0.199 (0.160)	0.026 (0.035)			−0.035 (0.124)	561.64	3.06
9	GPD-5	2.734 (0.179)	−0.003 (0.063)				−0.080 (0.137)	561.69	3.11
10	GPD-8	3.761 (0.826)	−0.201 (0.161)	0.007 (0.062)			−0.052 (0.121)	562.21	3.63
11	GPD-15	2.987 (0.209)	0.030 (0.036)	−0.840 (0.486)	0.012 (0.063)		−0.055 (0.118)	562.27	3.68
12	GPD-12	2.847 (1.027)	0.031 (0.219)	0.031 (0.036)	−0.890 (0.672)		−0.060 (0.120)	562.28	3.70
13	GPD-14	2.873 (1.020)	0.010 (0.218)	−0.845 (0.683)	0.015 (0.062)		−0.075 (0.119)	563.04	4.46
14	GPD-10	2.78 (0.189)	0.026 (0.035)	−0.007 (0.064)			−0.055 (0.142)	563.32	4.74
15	GPD-13	3.807 (0.831)	−0.201 (0.161)	0.025 (0.035)	0.004 (0.063)		−0.035 (0.124)	563.93	5.35
16	GPD-16	2.851 (1.027)	0.030 (0.219)	0.031 (0.036)	−0.905 (0.679)	0.012 (0.063)	−0.058 (0.121)	564.61	6.03

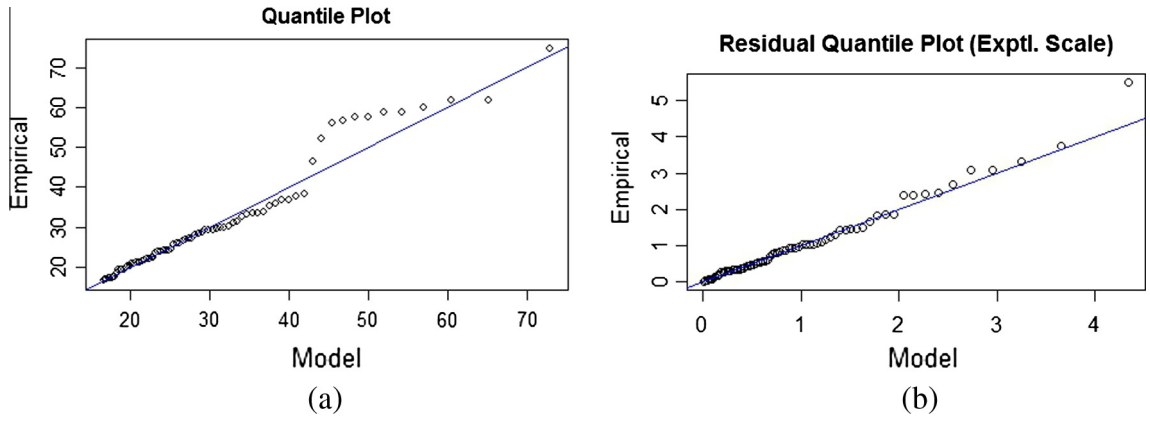

Fig. 18. The QQ plots of (a) GPD-1, (b) GPD-4 from non-monsoon 5 p.m. to 8 p.m. extreme rainfall.

rainfall events in this period and these rainfall events are separated by 20 h or more. Thus, no declustering is carried out for 5 p.m. to 8 p.m. non-monsoon rainfall. The 16 GPD models fitted with these extreme rainfall events are given in Table 19. The GPD-4 is found to be the best model for non-monsoon months' 5 p.m. to 8 p.m. extreme rainfall. The stationary model GPD-1 is ranked 2 and it is considerable based on Δ_i value. Unlike other rainfall, the difference between non-stationary best GPD model and stationary GPD model is very less for 5 p.m. to 8 p.m. non-monsoon rainfall. The QQ plots of GPD-1 and GPD-4 of 5 p.m. to 8 p.m. non-monsoon rainfall are shown in Fig. 18(a) and (b) respectively. The different Poisson model's performance for non-monsoon months' 5 p.m. to 8 p.m. extreme rainfall frequency with different physical covariates and their combinations are given in Table 20. Among 16 Poisson models, the P-3 is found to be the best model. The stationary model P-1 is ranked 9 and it is not even considerable based on Δ_i value.

Table 20
Poisson models' performance with **non-monsoon 5 p.m. to 8 p.m.** extreme rainfall. Models are sorted according to Δ_i value.

Rank	Model ID	λ_0 (SE)	λ_1 (SE)	λ_2 (SE)	λ_3 (SE)	λ_4 (SE)	AICc	Δ_i
1	P-3	−5.200 (0.149)	−0.065 (0.033)				917.81	0.00
2	P-6	−6.344 (0.900)	0.219 (0.169)	−0.063 (0.033)			918.10	0.29
3	P-10	−5.190 (0.149)	−0.067 (0.033)	−0.059 (0.053)			918.59	0.78
4	P-9	−5.314 (0.188)	−0.065 (0.033)	0.470 (0.445)			918.68	0.87
5	P-13	−6.374 (0.914)	0.227 (0.172)	−0.064 (0.033)	−0.060 (0.053)		918.82	1.01
6	P-15	−5.308 (0.189)	−0.067 (0.033)	0.489 (0.452)	−0.060 (0.053)		919.41	1.60
7	P-12	−6.289 (1.297)	0.207 (0.271)	−0.063 (0.033)	0.042 (0.722)		920.10	2.29
8	P-2	−6.305 (0.907)	0.241 (0.170)				920.18	2.37
9	P-1	−5.041 (0.115)					920.21	2.40
10	P-16	−6.304 (1.303)	0.211 (0.273)	−0.065 (0.033)	0.055 (0.726)	−0.060 (0.053)	920.82	3.01
11	P-4	−5.159 (0.164)	0.484 (0.453)				921.06	3.25
12	P-8	−6.342 (0.921)	0.251 (0.173)	−0.058 (0.055)			921.08	3.27
13	P-5	−5.028 (0.115)	−0.056 (0.055)				921.21	3.40
14	P-11	−5.150 (0.165)	0.501 (0.460)	−0.057 (0.055)			922.01	4.20
15	P-7	−6.371 (1.303)	0.256 (0.272)	−0.052 (0.733)			922.18	4.37
16	P-14	−6.404 (1.309)	0.265 (0.273)	−0.049 (0.737)	−0.058 (0.055)		923.08	5.27

Table 21
Most significant physical process/processes which are causing non-stationarity in extreme rainfall intensity and frequency.

Rainfall	Most significant physical covariate(s) causing non-stationarity in extreme rainfall intensity (stationary model)	Most significant physical covariate(s) causing non-stationarity in extreme rainfall frequency (stationary model)
Daily-monsoon rainfall	Global temperature anomaly with ENSO cycle (NC)	Urbanization (C)
Daily non-monsoon rainfall	ENSO cycle (NC)	Local temperature anomaly with global temperature anomaly (NC)
1 a.m. to 4 a.m. monsoon rainfall	Urbanization (NC)	Stationary
5 p.m. to 8 p.m. monsoon rainfall	ENSO cycle (NC)	Stationary
9 p.m. to 12 p.m. monsoon rainfall	Urbanization (NC)	ENSO cycle (NC)
5 p.m. to 8 p.m. non-monsoon rainfall	Global temperature anomaly (C)	Local temperature anomaly (NC)

Note: NC – not considerable; C – considerable.

6. Summary and conclusions

With the help of IMD hourly rainfall observations and APHRODITE high resolution daily gridded rainfall data, the changes in Hyderabad city rainfall are analyzed. Our analysis reveals that the monthly rainfall of urban area (Hyderabad city) is more during the monsoon months (June–August) when compared to surrounding non-urban areas. Further, during the monsoon months (June–August), the rainfall that occurred during 1 a.m. to 4 a.m., 5 p.m. to 8 p.m. and 9 p.m. to 12 a.m. has increased significantly. In particular, during the monsoon months, percentage rainfall that occurred between 1 a.m. and 4 a.m. has increased by 4.5% and nearly 1% increase in percentage rainfall that occurred between 5 a.m. and 8 a.m. Though the percentage rainfall that occurred between 9 p.m. and 12 a.m. is remains same, a significant increase in rainfall is observed. During non-monsoon months, maximum of 8.52% increase in percentage rainfall that occurred between 5 p.m. and 8 p.m. and maximum of 8.67% decrease in percentage rainfall that occurred between 9 p.m. and 12 a.m. is observed. The rainfall and percentage of rainfall that occurred in other time periods of non-monsoon months are nearly same. Further, with the help of various climate change detection indices, the changes in daily extreme rainfall, monsoon months' 1 a.m. to 4 a.m., 5 p.m. to 8 p.m. and 9 p.m. to 12 a.m. extreme rainfall and non-monsoon months' 5 p.m. to 8 p.m. extreme rainfall are analyzed and increasing trend in extreme rainfall intensity and frequency of these periods is observed.

In addition, to attribute the possible cause for the change in extreme rainfall, the extreme rainfall intensity is modelled with POT based non-stationary GPD and frequency is modelled using inhomogeneous Poisson distribution. The extreme rainfall value (threshold) is interpreted using MRL plots. The trend is incorporated as a covariate in the scale parameter (σ) of GPD and the rate parameter (λ) of the Poisson distribution. Four physical processes (i.e. Urbanization, ENSO cycle, local temperature change, and global warming) are used as covariates and based on these four covariates and their combinations, fifteen non-stationary models and one stationary model are constructed and the best model is chosen based on AICc value. The covariate(s) in the best chosen non-stationary statistical model is/are attributed as the most significant physical process/processes which causes non-stationarity in the series. Table 21 reveals the most significant physical process/processes which are causing non-stationarity in intensity and frequency of Hyderabad city extreme rainfall. Except, monsoon months' 1 a.m. to 4 a.m. and 5 p.m. to 8 p.m. extreme rainfall requency, all other extreme rainfall intensity and frequency are associated with one or two physical processes. It is also observed that, in most of the cases, the stationary model is not even considerable. In addition, it is observed that the MEI with lag 10 months is the best ENSO cycle indicator for monsoon months and SOI with 11 months lag is the best ENSO cycle indicator for non-monsoon months.

From the study results, it is observed that the non-stationarity in daily extreme rainfall of Hyderabad city is mostly associated with global processes, i.e. ENSO cycle and global warming and the non-stationarity in sub-daily (4-h) extreme rainfall is mostly associated with local processes, i.e. Urbanization and local temperature changes. The results of this study may help us to develop non-stationary Intensity–Duration–Frequency (IDF) relationship for urban infrastructural design. Further, the flood prediction in urban areas can be improved by incorporating attributed physical processes of this study.

Acknowledgements

This work is supported by Information Technology Research Academy (ITRA), Government of India under, ITRA-water grant ITRA/15(68)/water/IUFM/01. We also thank the India Meteorolog-

ical Department for providing rainfall and temperature data. Landsat satellite images are downloaded from the U.S. Geological Survey.

References

Agilan, V., Umamahesh, N.V., 2015. Effect of el Niño-southern oscillation (ENSO) cycle on extreme rainfall events of Indian urban area. In: Vellore, Proceedings of International Conference on Sustainable Energy and Built Environment, pp. 569–573.

Alexander, L.V. et al., 2006. Global observed changes in daily climate extremes of temperature and precipitation. J. Geophys. Res. 111, D05109: 1–22.

Allen, M.R., Ingram, W.J., 2002. Constraints on future changes in climate and the hydrologic cycle. Nature 419, 224–232.

Anderson, J.R., Hardy, E.E., Roach, J.T., Witmer, R.E., 2001. A Land Use and Land Cover Classification System for Use with Remote Sensor Data, Geological Survey Professional Paper 964. United States Government Printing Office, Washington.

Avei, M., Akyurek, Z., 2004. A Hierarchical Classification of Landsat TM Imagery for Landcover Mapping. Istanbul, Turkey, IAPRS, ISSN 1682-1750.

Berg, P., Moseley, C., Haerter, J.O., 2013. Strong increase in convective precipitation in response to higher temperatures. Nat. Geosci. 6, 181–185.

Burian, S.J., Shepherd, J.M., 2005. Effect of urbanization on the diurnal rainfall pattern in Houston. Hydrol. Process. 19, 1089–1103.

Burnham, K.P., Anderson, D.R., 2004. Multimodel inference: understanding AIC and BIC in model selection. Sociol. Meth. Res. 33, 261–304.

Cavanaugh, N.R., Gershunov, A., Panorska, A.K., Kozubowski, T.J., 2015. The probability distribution of intense daily precipitation. Geophys. Res. Lett. 42.

Changnon, S.A., Huff, F.A., Semonin, R.G., 1971. METROMEX: an investigation of inadvertent weather modification. Am. Meteorol. Soc. 52 (10), 958–967.

Cheng, L., Kouchak, A.A., Gilleland, E., Katz, R.W., 2014. Non-stationary extreme value analysis in a changing climate. Clim. Change 127, 353–369.

Coles, S., 2001. An Introduction to Statistical Modelling of Extreme Values. Springer, London.

Congalton, R.G., Green, K., 2009. Assessing the Accuracy of Remotely Sensed Data, second ed. CRC Press, New York.

DESA, 2010. World Urbanization Prospects: The 2009 Revision. United Nations, New York.

Emori, S., Brown, S.J., 2005. Dynamic and thermodynamic changes in mean and extreme precipitation under changed climate. Geophys. Res. Lett. 35, L17706.

Gibson, P.J., Power, C.H., 2000. Introductory Remote Sensing: Digital Image Processing and Applications. Routledge, London.

Indu, J., Kumar, D.N., 2014. Evaluation of TRMM precipitation products over Indian subcontinent. Hyderabad, The International Archives of the Photogrammetry, Remote Sensing and Spatial Information Sciences, pp. 355–358.

IPCC, 2013. Climate Change 2013: The Physical Science Basis. Contribution of Working Group I to the Fifth Assessment Report of the Intergovernmental Panel on Climate Change. Cambridge University Press, Cambridge, United Kingdom and New York.

Katz, R.W., 2013. Statistical methods for nonstationary extremes. In: Kouchak, A.A. et al. (Eds.), Extremes in a Changing Climate: Detection, Analysis and Uncertainty. Springer, London, pp. 15–37.

Katz, R.W., Parlange, M.B., Naveau, P., 2002. Statistics of extremes in hydrology. Adv. Water Resour. 25 (8), 1287–1304.

Kenyon, J., Hegerl, G.C., 2010. Influence of modes of climate variability on global precipitation extremes. J. Clim. 23 (23), 6248–6262.

Khaliq, M.N. et al., 2006. Frequency analysis of a sequence of dependent and/or non-stationary hydro-meteorological observations: a review. J. Hydrol. 329, 534–552.

Kishtawal, C.M. et al., 2009. Urbanization signature in the observed heavy rainfall climatology over India. Int. J. Climatol. 30 (13).

Krishnamurthy, V., Shukla, J., 2000. Intraseasonal and interannual variability of rainfall over India. J. Clim. 13, 4366–4377.

Kunkel, K.E. et al., 2013. Probable maximum precipitation and climate change. Geophys. Res. Lett. 40, 1402–1408.

Lei, M. et al., 2008. Effect of explicit urban land surface representation on the simulation of the 26 July 2005 heavy rain event over Mumbai, India. Atmos. Chem. Phys. 8, 5975–5995.

Li, C. et al., 2014. Comparison of classification algorithms and training sample sizes in urban land classification with landsat thematic mapper imagery. Remote Sens. 6, 964–983.

Lu, D., Weng, Q., 2007. A survey of image classification methods and techniques for improving classification performance. Int. J. Remote Sens. 28 (5), 823–870.

Martins, E.S., Stedinge, J.R., 2001. Generalized maximum likelihood Pareto-Poisson estimators for partial duration series. Water Resour. Res. 37 (10), 2551–2558.

Miao, S., Chen, F., Fan, Q.L., 2011. Impacts of urban processes and urbanization on summer precipitation: a case study of heavy rainfall in Beijing on 1 August 2006. J. Appl. Meteorol. Climatol. 50 (4), 806–825.

Min, S.K., Zhang, X., Zwiers, F.W., Hegerl, G.C., 2011. Human contribution to more-intense precipitation extremes. Nature 470, 378–381.

Mondal, A., Mujumdar, P.P., 2015. Modeling non-stationarity in intensity, duration and frequency of extreme rainfall over India. J. Hydrol. 521, 217–231.

NASA, L.P., 1972. Landsat MSS scene LM11540481972352AAA05 level1T. USGS, Sioux Falls.

NASA, L.P., 1981. Landsat MSS scene LM31550481981287AAA05 level1T. USGS, Sioux Falls.

NASA, L.P., 1989. Landsat TM scene LT51440481989053ISP00 level1T. USGS, Sioux Falls.

NASA, L.P., 1994. Landsat TM scene LT51440481994115ISP00 level1T. USGS, Sioux Falls.

NASA, L.P., 2000. Landsat ETM scene LE71440482000060SGS00 level1T. USGS, Sioux Falls.

NASA, L.P., 2003. Landsat ETM scene LE71440482003020SGS00 level1T. USGS, Sioux Falls.

NASA, L.P., 2006. Landsat TM scene LT51440482006100BKT00 level1T. USGS, Sioux Falls.

NASA, L.P., 2010. Landsat TM scene LT51440482010111BKT01 level1T. USGS, Sioux Falls.

NASA, L.P., 2013. Landsat OLI-TIRS scene LC81440482013359LGN00 level1T. USGS, Sioux Falls.

Nelder, J.A., Mead, R., 1965. A simplex algorithm for function minimization. Comput. J. 7, 308–313.

Nogaj, M., Parey, S., Castelle, D.D., 2007. Non-stationary extreme models and a climatic application. Nonlin. Process. Geophys. 14, 305–316.

Peel, M.C., Finlayson, B.L., McMahon, T.A., 2007. Updated world map of the Koppen-Geiger climate classification. Hydrol. Earth Syst. Sci. 11, 1633–1644.

Rajeevan, M., Bhate, J., 2009. A high resolution daily gridded rainfall data set (1971–2005) for mesoscale meteorological studies. Curr. Sci. 96 (4), 558–562.

Revadekar, J.V., Kulkarni, A., 2008. The El Nino-Southern Oscillation and winter precipitation extremes over India. Int. J. Climatol. 28, 1445–1452.

Scarrott, C.J., MacDonald, A., 2012. A review of extreme value threshold estimation and uncertainty quantification. REVSTAT – Stat. J. 10 (1), 33–59.

Shepherd, J.M., Burian, S.J., 2003. Detection of urban-induced rainfall anomalies in a major coastal city. Earth Interact. 7, 4:1–17.

Shepherd, J.M., Pierce, H., Negri, A.J., 2001. Rainfall modification by major urban areas: observations from spaceborne rain radar on the TRMM satellite. J. Appl. Meteorol. 41, 689–701.

Stephenson, D.B., 2008. Definition, diagnosis, and origin of extreme weather and climate events. In: Climate Extremes and Society. Cambridge University Press, Cambridge.

Sugahara, S., Rocha, R.P., Silveira, R., 2009. Non-stationary frequency analysis of extreme daily rainfall in Sao Paulo, Brazil. Int. J. Climatol. 29, 1339–1349.

Trenberth, K.E., 2011. Changes in precipitation with climate change. Clim. Res. 47, 123–138.

Trenberth, K.E., Dai, A., Rasmussen, R.M., Parsons, D.B., 2003. The changing character of precipitation. Bull. Am. Meteorol. Soc. 84 (9), 1205–1217.

UNFPA, 2007. State of World Population 2007: Unleashing the Potential of Urban Growth. s.l., UNFPA.

Villafuerte, M.Q., Matsumoto, J., 2015. Significant influences of global mean temperature and ENSO on extreme rainfall in Southeast Asia. J. Clim. 28, 1905–1919.

Wolter, K., Timlin, M.S., 1998. Measuring the strength of ENSO events: how does 1997/98 rank? Weather 53 (9), 315–324.

XiQuan, W., ZiFa, W., YanBin, Q., Hu, G., 2009. Effect of urbanization on the winter precipitation distribution in Beijing area. Sci. China Ser. D-Earth Sci. 52 (2), 250–256.

Xu, L. et al., 2015. Precipitation trends and variability from 1950 to 2000 in arid lands of Central Asia. J. Arid Land 7 (4), 514–526.

Yang, L., Tian, F., Niyogi, D., 2015. A need to revisit hydrologic responses to urbanization by incorporating the feedback on spatial rainfall patterns. Urban Clim. 12, 128–140.

Yatagai, A. et al., 2012. APHRODITE: constructing a long-term daily gridded precipitation dataset for Asia based on a dense network of rain gauges. Am. Meteorol. Soc., 1401–1415

Zelle, H., Appeldoorn, G., Burgers, G., Oldenborgh, G.J., 2004. The relationship between sea surface temperature and thermocline depth in the Eastern Equatorial Pacific. J. Phys. Oceanogr. 34, 643–655.

Zeng, X., Zwires, F.W., 2013. Statistical indices for the diagnosing and detecting changes in extremes. In: Extremes in a Changing Climate: Detection, Analysis and Uncertainty. Springer, pp. 1–14, s.l.

Zhang, C.L. et al., 2009. Impacts of urban expansion and future green planting on summer precipitation in the Beijing metropolitan area. J. Geophys. Res. 114, D02116:1–26.

Zhang, X. et al., 2011. Indices for monitoring changes in extremes based on daily temperature and precipitation data. WIREs: Clim. Change 2 (6), 851–870.

Zhang, X., Wang, J., Zwiers, F.W., 2010. The influence of large-scale climate variability on winter maximum daily precipitation over North America. J. Clim. 23, 2902–2915.

Zhang, Y. et al., 2014. Urbanization and rainfall variability in the Beijing Metropolitan region. J. Hydrometeorol. 15 (6), 2219–2235.